ABSTRACT

Title of Thesis:	DETERMINATION OF ROUND EXIT VELOCITY USING FIBER BRAGG GRATING SENSORS
Degree Candidate:	Arvind Ramaswamy Aiyar,
Degree and Year:	Master of Science, 2004
Thesis Directed By:	Professor Christopher C. Davis Department of Electrical & Computer Engineering

Optical fiber sensing technology has found widespread applications in smart structures and intelligent engineering systems. In particular, the use of fiber Bragg grating sensors for strain, temperature and pressure measurement has been an area of active research in the past decade.

In this thesis, an experimental technique to measure the exit velocity of projectiles in field-deployed gun barrels is presented. In-fiber Bragg grating sensors are used to monitor the onset of propagating hoop strain waves accompanying the passage of rapidly moving projectiles. A fixed optical filter is used for providing temperature compensation and enable high-speed data acquisition. The elapsed time information extracted from the resulting strain waves is used to estimate the round exit velocity (REV). An approach based on short-time Fourier analysis and cross-correlation has

been developed to accurately measure the REV to within 1% error. Results from live-fire tests are presented and compared to reference velocity data.

DETERMINATION OF ROUND-EXIT VELOCITY USING FIBER BRAGG GRATING SENSORS

By

Arvind Ramaswamy Aiyar

Thesis or Dissertation submitted to the Faculty of the Graduate School of the
University of Maryland, College Park, in partial fulfillment
of the requirements for the degree of
Master of Science
2004

Advisory Committee:
Professor Christopher C. Davis, Chair
Professor Julius Goldhar
Professor Thomas E. Murphy

Acknowledgements

I owe this work to a lot of people who have been a constant source of encouragement and support to me for the duration of this project.

First and foremost, I am deeply grateful to my advisor, Dr. Chris Davis for giving me the opportunity to be a part his research group and work on this project. I would like to thank him for his thoughtful insights and continuous feedback at every stage of this work. I have learned a lot from his conceptual and thought-provoking approach to every problem which has made my experience both fruitful and enjoyable. I want to thank Dr. Thomas Murphy and Dr. Julius Goldhar for agreeing to serve on my thesis committee.

I am also thankful to the people at TechnoSciences Inc. especially Dr. Gilmer Blankenship, Mr. Chris LaVigna and Dr. Peter Chen for providing me with the opportunity and the facilities to conduct my experiments, and to Patrick Kimvilakani and Gaurav Bajpai who were ever ready to lend a helping hand. I especially owe a whole lot to Justin Bowlus for being an excellent guide and a great friend. I have a learnt an enormous amount from him: from system design, machining practices, presentation skills and even a bit about philosophy!

I am also extremely grateful and lucky to have Sukanya by my side. Without her presence and her 'motivational speeches', this work would not have materialized.

Finally, I would also like to thank my parents and Avishek for their love and support from thousands of miles away, which has always kept me going in whatever I do.

Table of Contents

List of Figures

Chapter 1: Introduction

The last three decades have seen a rapid advancement in the area of optical fiber technology and applications, essential in modern-day telecommunication systems. The telecommunication revolution became a route for progress in this technology, as mass production techniques coupled with technical improvements resulted in superior performance at lower costs than those of alternative approaches. As an offshoot of this revolution emerged another one as a result of the combination of fiber optic telecommunication product outgrowths with optoelectronic devices, creating fiber optic sensors.

A particular area where fiber optic sensors have found widespread usage is in smart structures and intelligent systems wherein their manifold advantages -- freedom from electromagnetic interference, wide bandwidth, high sensitivity, light weight, compactness, geometric versatility and economy --- have proved suitable for sensing applications, particularly in high temperature and other harsh environments. A few examples include fatigue tracking in fighter aircraft [28], structural health monitoring in space shuttles, strain sensing in field deployed naval and military armaments and, in recent times, in biomedical applications for monitoring ventilatory movements in the human body [26].

Within the ambit of fiber optic sensors, in-fiber Bragg grating sensors for strain and temperature measurement have generated significant interest in the technical community [15, 16, 26]. An important application in the military domain can be found in the development of so-called smart weapons systems. The next generation of

weapons systems demands greater target accuracy, reduced wear and tear, longer lifetimes and a greater degree of automation. An important metric for gun barrel performance is the round-exit velocity (REV) of the projectile before it exits the barrel. The REV is also critical in understanding the interior ballistics of the weapons system. Therefore, an accurate method to measure the REV would prove useful for determining barrel lifetime, improve health monitoring and also provide automatic, real-time fuse-setting features. Current REV measurement schemes have several inherent disadvantages which make them difficult for deployment in field environments. In this study, we propose an REV measurement technique based on Fiber Bragg grating sensors that can provide better REV estimates, be easily deployed and also be incorporated into real-time fuse programming systems.

A fiber Bragg grating sensor consists of a periodic modulation of the refractive index in the core of the optical fiber. Incident light can be coupled forwards (transmission) or backwards (reflection) due to diffraction at the grating structure. An interesting feature of Bragg gratings is that the reflection spectrum is sharply peaked with a well-defined center wavelength, which shifts linearly in response to external strain or temperature effects. We utilize this property to compute the round-exit velocity of a projectile traveling through a gun barrel, while it is still in bore, by detecting the traveling hoop strain wave accompanying the projectile.

Chapter 2 of this thesis introduces the fundamentals of fiber Bragg gratings. In order to analyze the physics of Bragg gratings, a brief mathematical model is presented. Two fiber grating fabrication techniques and general characterization methods are

briefly discussed. The spectral characteristics, especially in response to strain and temperature are also described.

Chapter 3 reviews the interior ballistics of military armament systems. The various methods to determine the exit velocity of the projectile are analyzed in order to clearly illustrate the advantages of fiber optic sensing schemes over existing mechanisms.

Chapter 4 provides the detailed description and analysis of our REV measurement system. Operational principles, system design specifications and results from live-fire tests are presented. A signal processing algorithm based on short-time Fourier analysis and cross-correlation to compute the exact REV is also discussed.

Chapter 5 concludes the thesis with a summary of the research work. Some suggestions for future work are also provided.

Chapter 2: Fiber Bragg Gratings

2.1 Introduction

A Fiber Bragg grating (FBG) is an optical fiber in which the refractive index in the core is perturbed, forming a periodic or quasi-periodic index modulation profile. Figure 2.1 shows a schematic profile of the structure of a typical Bragg grating.

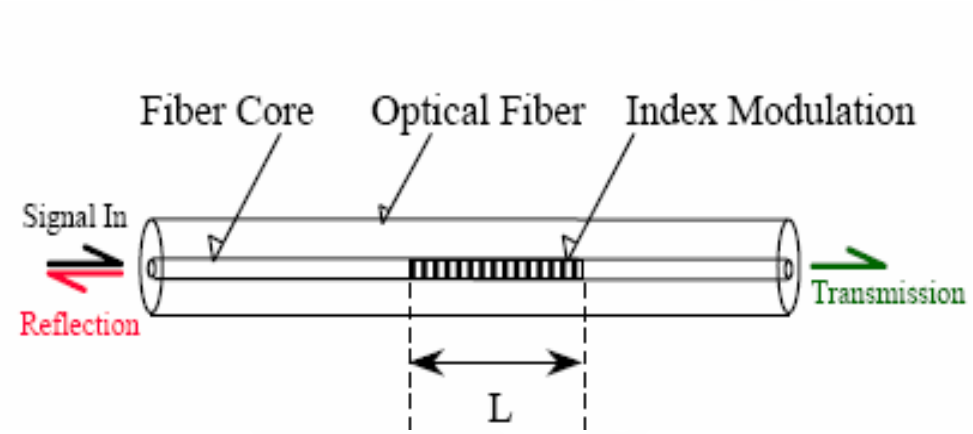

Figure 2.1 The refractive index structure in a typical fiber grating

The physical property that is responsible for the index change in an optical fiber is called photosensitivity. It has been found that germanium doped silica glass has a strong absorption band centered around 5eV, which corresponds to wavelengths in the ultra-violet (UV) region. The process of refractive index change in germanium doped silica glass through UV light absorption is described by the Kramers-Kronig relations [29]. This phenomenon is known as photosensitivity and is different from photorefractivity and the photochromic effect. Hill *et al* [4] reported the first in-fiber Bragg grating in 1978 in germanium doped fibers. The relative change in refractive

index can be controlled by the material properties of the optical fiber, by the dose of UV light exposure and by photosensitization procedures (e.g. using dopants or loading with hydrogen). The variation can either be perpendicular to the axis of the fiber or at an angle [25]; different orientations of the fiber gratings enable various properties.

In a uniform fiber grating profile, periodic index planes are formed perpendicular to the longitudinal axis of the fiber, analogous to diffraction planes in a crystalline solid. When light is guided through a fiber grating, it is scattered at each diffraction plane. In general, the reflected light will be out of phase and will tend to cancel, except at those wavelengths which satisfy the Bragg resonance condition. In this case, light at these wavelengths will be scattered in phase at successive index planes. The grating thus couples the energy from the forward propagating wave to a backward propagating reflected wave. In a periodic structure, the Bragg condition is satisfied for a narrow set of wavelengths resulting in a narrow band of reflected light with a sharp reflectance peak. The center wavelength that satisfies the Bragg condition is called the Bragg wavelength.

In this chapter, we will review the mathematical theory and the physics of fiber Bragg gratings, which will be helpful in modeling them. General characterization methods and fiber grating fabrication techniques are also briefly discussed. Finally, we review the behavior of Bragg gratings under the influence of strain and temperature.

2.2 Mathematical model of Fiber Bragg gratings

2.2.1 Resonant Wavelength for grating diffraction

In order to better understand the analysis of Bragg gratings, it is helpful to review the qualitative picture of the basic interactions of interest [7]. An FBG is nothing but an optical diffraction grating. For a light wave incident on the grating at an angle θ_1 (Figure 2.2), the effect can be described by the grating equation [17]:

$$n\sin\theta_2 = n\sin\theta_1 + m\frac{\lambda}{\Lambda} \tag{2.1}$$

where n is the refractive index of the medium, θ_2 is the angle of the diffracted wave, Λ is the period of the grating and m is the diffraction order. The equation describes the angles where constructive interference occurs, but can nevertheless be used to determine the wavelength at which the fiber grating most efficiently couples light between two modes.

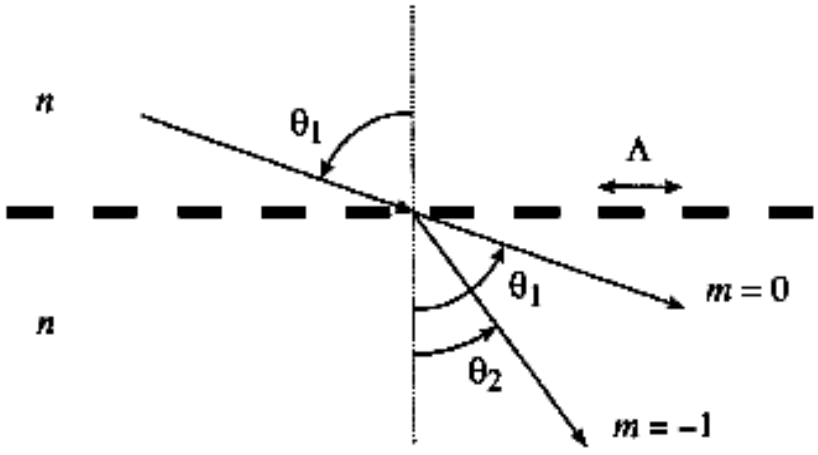

Figure 2.2 Diffraction of an incident light wave by a grating

In a fiber Bragg grating, light energy is coupled between electromagnetic waves traveling in opposite directions. In other words, it is a reflection grating and we observe the light spectrum in reflection, as opposed to transmission or long period gratings where mode coupling is co-directional.

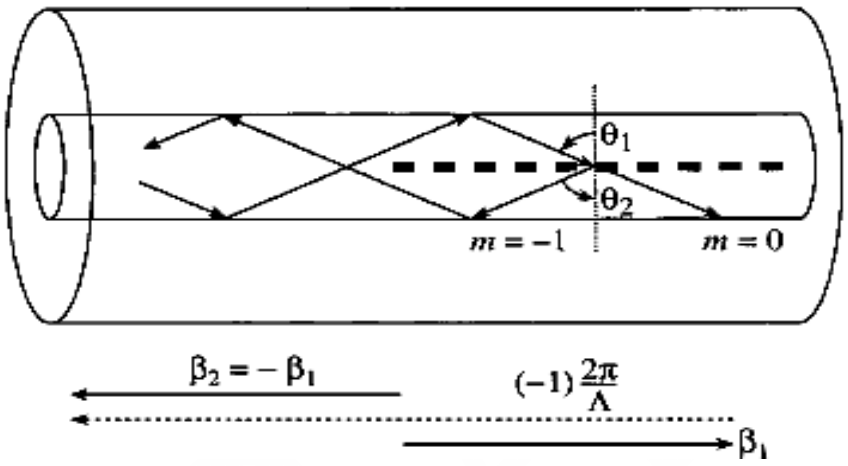

Figure 2.3 Reflection of core modes in a Bragg grating

Fig 2.3 illustrates a simple Bragg grating in which light energy is coupled from a mode incident at a bounce angle of θ_1 into the same mode traveling in the opposite direction at an angle $\theta_2 = -\theta_1$. Using n_{co} and n_{cl} to denote the core and cladding refractive indices respectively, we can rewrite Eq. 2.1 above in terms of the mode propagation constant $\beta = (2\pi / \lambda) n_{eff}$, where $n_{eff} = n_{co} \sin\theta$ as :

$$\beta_2 = \beta_1 + m\frac{2\pi}{\Lambda} \tag{2.2}$$

Considering the dominant first-order diffraction in the fiber grating for which m = -1, and realizing that $\beta_2 < 0$, we determine that the resonant wavelength condition for reflection of a mode of index n_{eff1} into a mode of index n_{eff2} is:

$$\lambda = (n_{eff1} + n_{eff2})\Lambda \tag{2.3}$$

If the two modes are identical, then we arrive at the result for the Bragg reflection condition as:

$$\lambda_B = 2n_{eff}\Lambda \tag{2.4}$$

2.2.2 Coupled Mode Theory

There are various methods to model Fiber Bragg grating structures, but the one widely discussed in literature is based on coupled mode theory [6, 7, 8]. Coupled-mode theory is a good tool for obtaining quantitative information about the diffraction efficiency and spectral dependence of fiber gratings. Coupled-mode theory is straightforward, intuitive, and it accurately models the optical properties of most fiber gratings of interest. A detailed derivation of the coupled-mode formalism can be found in [29] and [10]. In this section, we will go over the results of the formalism as illustrated in [7].

In a fiber grating, the geometrical variations in the fiber core are nothing but perturbations to the effective refractive index, n_{eff}, of the guided mode(s). We assume that this perturbation can be described by:

$$\delta n_{eff}(z) = \bar{\delta} n_{eff}(z)\left\{1 + v\cos\left[\frac{2\pi}{\Lambda}z + \phi(z)\right]\right\} \tag{2.5}$$

where $\overline{\delta n}_{eff}$ is the "dc" index change spatially averaged over a grating period, v is the fringe visibility of the index change, Λ is the nominal grating period, and $\phi(z)$ describes the grating chirp.

In the ideal-mode approximation to coupled-mode theory, we assume that the transverse component of the electric field, E_t can be expressed as a superposition of the ideal modes (i.e. without grating perturbation) notated by j:

$$\vec{E}_t(x,y,z,t) = \sum_j \left[A_j(z)e^{(i\beta_j z)} + B_j(z)e^{(-i\beta_j z)} \right].\vec{e}_{jt}(x,y)e^{-i\omega t} \tag{2.6}$$

where $A_j(z)$ and $B_j(z)$ are slowly varying amplitudes of the jth mode traveling in the $+z$ and $-z$ directions. The transverse modes $\vec{e}_{jt}(x,y)$ may describe radiation modes or cladding modes. In general, these modes are orthogonal and do not exchange energy. However, in the presence of a dielectric perturbation, they are coupled according to:

$$\frac{dA_j}{dz} = i\sum_k \left[A_k(K^t_{kj} + K^l_{kj})e^{\left[i(\beta_k-\beta_j)z\right]} + i\sum_k B_k(K^t_{kj} - K^l_{kj})e^{\left[-i(\beta_k+\beta_j)z\right]} \right] \tag{2.7}$$

$$\frac{dB_j}{dz} = -i\sum_k \left[A_k(K^t_{kj} - K^l_{kj})e^{\left[i(\beta_k+\beta_j)z\right]} - i\sum_k B_k(K^t_{kj} + K^l_{kj})e^{\left[-i(\beta_k-\beta_j)z\right]} \right] \tag{2.8}$$

where $K^t_{kj}(z)$ is the transverse coupling coefficient between modes k and j given by:

$$K^t_{kj}(z) = \frac{\omega}{4}\iint_{\infty} dxdy\Delta\varepsilon(x,y,z)\vec{e}_{kt}(x,y).\vec{e}^{*}_{jt}(x,y) \tag{2.9}$$

Here, $\Delta\varepsilon$ is the small perturbation $\Delta\varepsilon \approx 2n\delta n$ when $\delta n << n$. The longitudinal coefficient $K^l_{kj}(z)$ is usually $<< K^t_{kj}(z)$ and is usually ignored.

If we define two new coefficients

$$\sigma_{kj}(z) = \frac{\omega n_{eff}}{2} \bar{\delta} n_{eff}(z) \iint_{\infty} dxdy \vec{e}_{kt}(x,y).\vec{e}^{*}_{jt}(x,y) \tag{2.10}$$

$$\kappa_{kj}(z) = \frac{v}{2} \sigma_{kj}(z) \tag{2.11}$$

where σ_{kj} is a "dc" averaged coupling coefficient and κ_{kj} is an "AC" averaged coupling coefficient, then the general coupling coefficient can be written as:

$$K^{t}_{kj}(z) = \sigma_{kj}(z) + 2\kappa_{kj}(z)\cos\left[\frac{2\pi}{\Lambda} z + \phi(z)\right] \tag{2.12}$$

2.2.3 Bragg Grating spectra

The basic equations 2.7 – 2.12 above can be used to describe the spectrum of fiber Bragg gratings. The theory of fiber Bragg gratings is developed by considering propagation of electromagnetic waves as guided modes in the optical fiber. In this analysis, we consider only periodic index gratings in the fiber core, which will be the sensor of interest in our system. We will assume that the fiber is lossless and single mode in the wavelength range of interest. In other words, we consider only one forward and one backward propagating mode. Moreover, we assume that the fiber is weakly guiding, i.e. the difference between the refractive indices in the core and the cladding is very small.

Near the wavelength at which mode coupling occurs, we can use the "synchronous approximation" [10], and neglect terms in Eqs. 2.7 and 2.8 which have a oscillating z dependence, which results in :

$$\begin{aligned} \frac{dR}{dz} &= i\hat{\sigma}R(z) + i\kappa S(z) \\ \frac{dS}{dz} &= -i\hat{\sigma}S(z) - i\kappa^* R(z) \end{aligned} \tag{2.13}$$

where $R \equiv A(z)exp(i\delta z - \varphi/2)$ and $S \equiv B(z)exp(-i\delta z + \varphi/2)$.

κ is the "AC" coupling coefficient as defined earlier while $\hat{\sigma}$ the "dc" self-coupling coefficient is:

$$\hat{\sigma} \equiv \delta + \sigma - \frac{1}{2}\frac{d\phi}{dz} \tag{2.14}$$

Here, σ is the "dc" coupling coefficient defined in Eq. 2.10 earlier, $\frac{1}{2}\, d\varphi/dz$ is the grating chirp and δ is the detuning which is defined as:

$$\delta \equiv \beta - \frac{\pi}{\lambda} = \beta - \beta_B = 2\pi n_{eff}\left(\frac{1}{\lambda} - \frac{1}{\lambda_B}\right) \tag{2.15}$$

where $\lambda_B = 2n_{eff}\Lambda$ is the familiar "target wavelength" defined by the Bragg reflection condition.

For a single mode Bragg reflection grating, the following relations hold [7]:

$$\begin{aligned} \sigma &= \frac{2\pi}{\lambda}\bar{\delta}n_{eff} \\ \kappa = \kappa^* &= \frac{\pi}{\lambda}v\bar{\delta}n_{eff} \end{aligned} \tag{2.16}$$

Further, for a uniform grating along z, $d\varphi/dz = 0$, $\bar{\delta} n_{eff}$ is constant and thus κ, σ and $\hat{\sigma}$ are constants. Hence, Eqs. 2.13 are coupled first-order differential equations with constant coefficients.

2.2.4 Analytical solutions

An analytical solution to the coupled-mode equations can be found using appropriate boundary conditions. For a grating length L, we assume a forward propagating wave from z =-∞ and no backward-propagating wave exists for $z \geq L/2$. This leads to the following boundary conditions:

$$\begin{aligned} R(-L/2) &= 1 \\ S(L/2) &= 0 \end{aligned} \tag{2.17}$$

Thus, we can express the grating reflection coefficients, ρ and R:

$$\begin{aligned} \rho &= \frac{-\kappa \sinh\left(\sqrt{\kappa^2 - \hat{\sigma}^2} L\right)}{\hat{\sigma} \sinh\left(\sqrt{\kappa^2 - \hat{\sigma}^2} L\right) + i\sqrt{\kappa^2 - \hat{\sigma}^2} \cosh\left(\sqrt{\kappa^2 - \hat{\sigma}^2} L\right)} \\ R &= \left|\rho\right|^2 = \frac{\sinh^2\left(\sqrt{\kappa^2 - \hat{\sigma}^2} L\right)}{\cosh^2\left(\sqrt{\kappa^2 - \hat{\sigma}^2} L\right) - \frac{\hat{\sigma}^2}{\kappa^2}} \end{aligned} \tag{2.18}$$

Figure 2.4 shows the spectral reflectance for uniform gratings plotted versus the wavelength for varying κL. For a fixed length, larger value of κL indicates deeper modulation, and the power reflectance and width increase with greater modulation index.

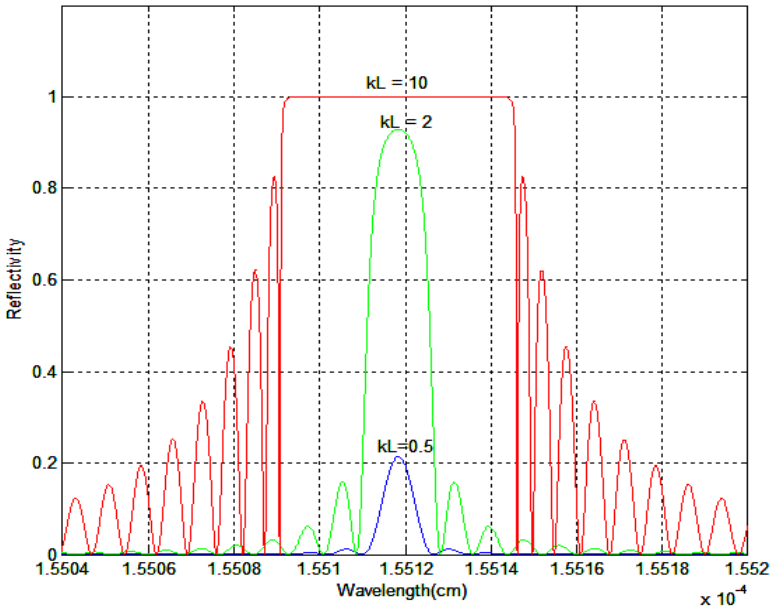

Figure 2.4 Simulation results for the reflectivity of an FBG
(L=1cm, n_{eff}=1.447, Λ=0.536μm)

The peak wavelength in the above reflection spectrum, λ_{max} occurs when $\hat{\sigma}=0$ and is given by:

$$\lambda_{\max} = \left(1 + \frac{\bar{\delta} n_{eff}}{n_{eff}}\right)\lambda_B \tag{2.19}$$

And, therefore the maximum reflectance is (from Eq. 2.18):

$$R_{\max} = \tanh^2(\kappa L) \tag{2.20}$$

2.3 Fabrication of periodic gratings in optical fibers

The fabrication of index gratings in optical fibers is initiated by photosensitizing the fiber core. Conventional optical fiber is made out of germanium doped silica glass and is photosensitive in the 240nm-250nm wavelengths [4]. Generally, the photosensitivity of the fiber is enhanced by hydrogenation [24] before UV irradiation.

In a typical germanium monomode fiber irradiated by laser intensities of 100-1000mJ/cm^2, a refractive index change Δn of magnitude 10^{-5}- 10^{-3} can be produced. Techniques like "hydrogen loading" can enhance the Δn to as high as 10^{-2}. Figure 2.5 shows the core refractive index profile of a typical germanium monomode fiber.

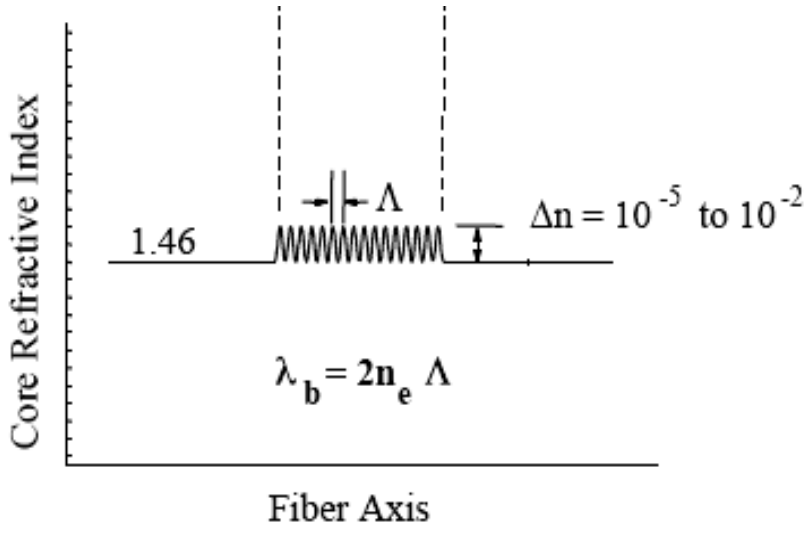

Figure 2.5 Typical grating structure for a germanium monomode fiber

The physical mechanisms underlying photosensitivity are not very well understood but are associated with the color centers in glassy materials. For example, UV photoexcitation of oxygen-vacancy-defect states [6] in Ge-SiO_2 fiber forms deficiency centers that contribute to the index change. The net result of the photoinduced changes is a permanent change in the refractive index of the glassy material at wavelengths far removed from the wavelength of the irradiating ultraviolet light.

This formation of permanent gratings in an optical fiber was first demonstrated by Hill *et al.* in 1978 [4] when they launched intense Argon-ion laser radiation into a

germanium-doped fiber and observed that after several minutes, an increase in the reflected light intensity occurred which grew until almost all the light was reflected back from the fiber. Spectral measurements, done indirectly by strain and temperature tuning of the fiber grating, confirmed that a very narrowband Bragg grating filter had been formed over the entire 1-m length of fiber. However, these 'Hill gratings' functioned only at visible light wavelengths close to the wavelength of the writing light. Subsequently, Meltz *et al.* [5] showed that this radiation could be made much more effective using the single-photon process to produce gratings capable of reflecting light at any wavelength.

There are two main methods to inscribe fiber gratings, a two-beam interference method and a phase mask method, which are described below.

2.3.1 Two-beam interference method for fabrication of Bragg gratings

The interferometric method for inscribing fiber gratings is an offshoot of the transverse holographic technique demonstrated by Meltz *et al.* [5]. In this method, two overlapping ultraviolet beams are made to interfere in a prescribed angle to produce an interference pattern. A cylindrical lens is used to focus the laser beam and obtain a high optical power density.

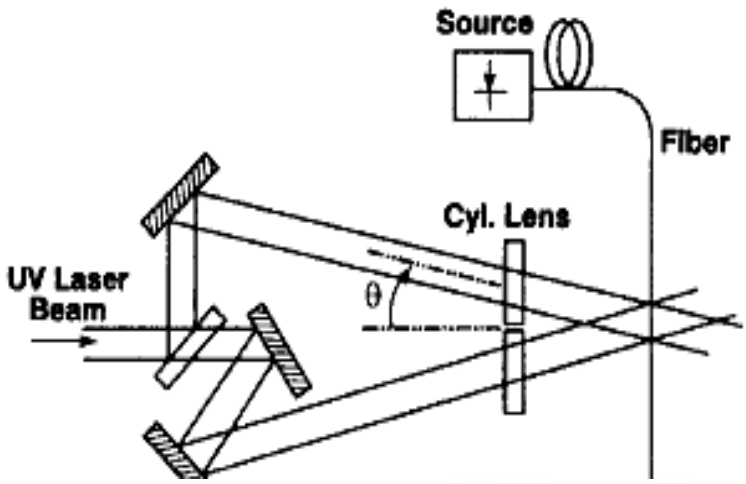

Figure 2.6 Two beam interferometer arrangement for writing FBGs

The mutual angle of interference (θ) is varied according to:

$$\Lambda = \frac{\lambda_{UV}}{2n_{UV}\sin(\theta/2)} \tag{2.21}$$

where Λ is the grating period, λ_{UV} is the wavelength of the UV light and n_{UV} is the refractive index of the fiber at the UV wavelength. The Bragg wavelengths of the grating are determined from Eq. 2.4. The interferometric method has the advantage that Bragg gratings could be photoimprinted in the fiber core without removing the glass cladding, as it is transparent to ultraviolet light. Further, the grating period depends simply on the mutual interference angle (θ) which offers a wide wavelength selectability range. However, this method has the disadvantage of requiring highly coherent sources and a very stable setup without any external disturbances.

2.3.2 Phase mask method for fabrication of Bragg gratings

The phase mask technique has largely superseded the holographic and the interferometric methods for grating fabrication [6]. A phase mask is a diffractive optical element made by etching grating patterns on fused silica substrates using standard photolithographic techniques. The shape of the periodic pattern approximates a square wave profile. The optical fiber is placed almost in contact with the corrugations of the phase mask as shown in Figure 2.7.

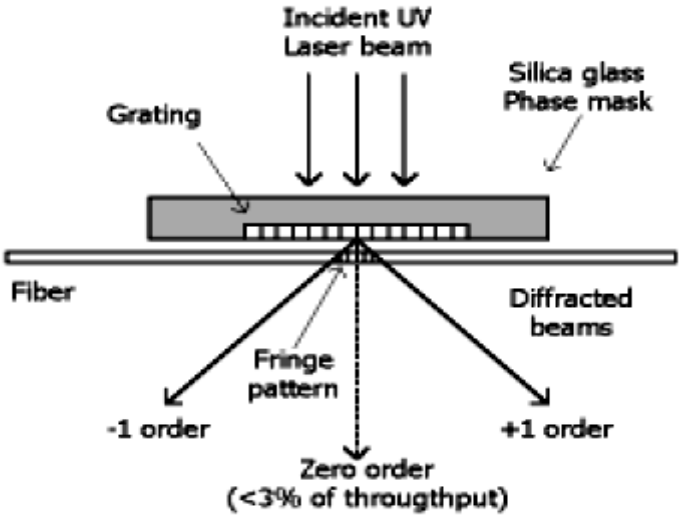

Figure 2.7 A schematic of fiber grating inscription using a phase mask

Ultraviolet light incident normally to the phase mask passes through and is diffracted by the periodic corrugations, creating an interference pattern. Normally, most of the diffracted light is contained in the 0, +1 and -1 diffracted orders. However, the phase mask is designed to suppress (< 3-5%) the diffraction into the zeroth order and maximize the first order diffraction efficiencies (~40%) by controlling the depth of the corrugations.

For normal incidence, the grating period (Λ) and the phase mask period (Λ_{pm}) is related by:

$$\Lambda = \Lambda_{pm} / 2 \tag{2.22}$$

The phase mask technique has the advantage of greatly simplifying the manufacturing process for Bragg gratings, yet yielding gratings with high performance. It is mechanically robust and does not require highly coherent light. However, it has the drawback of not being able to offer a wide wavelength tuning capability.

2.4 External characteristics of fiber Bragg gratings

Monitoring the spectral (internal) characteristics of Bragg gratings helps us investigate the spectral profile of the Bragg resonance away from the peak wavelength (reflection spectrum) or the strength of the grating (transmission spectrum). Figure 2.8 shows the reflection spectrum of an FBG with a sharply peaked Bragg wavelength at 1547.4 nm.

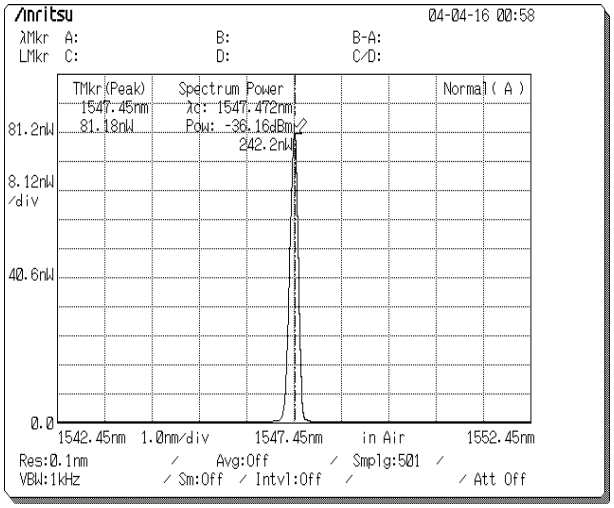

Figure 2.8 Reflection spectrum of a fiber Bragg grating sensor

However, the external characteristics primarily influence their use as sensors. The center wavelength of fiber Bragg grating's reflection spectrum is a function of the grating period and the fiber refractive index (Eq. 2.4). Therefore, any change in the fiber properties, such as strain, temperature or polarization, which varies the modal index or grating pitch will result in a shift in the center wavelength. The grating is an intrinsic sensor which changes the spectrum of an incident signal by coupling energy to other fiber modes. In the simplest case, the incident wave is coupled to the same counterpropagating mode and is reflected. Any external perturbation, both due to strain or temperature, is manifested by a wavelength shift and can be used as a direct measure of the strain or temperature.

2.4.1 Strain sensitivity

The strain response of the grating is caused by fractional changes to the grating period due to the actual elongation of the fiber, which is in turn manifested by a change in the refractive index of the fiber. This is called the photoelastic effect. In general, a grating has different sensitivities for axial and radial strains. In this research, both axial and radial strains are considered. However, assuming that the relationship between the axial and radial strain is known, we can theoretically model the wavelength shift in terms of the overall sensitivity of the Bragg grating to the longitudinal strain.

We can develop a detailed approach [18] to model the longitudinal strain sensitivity by revisiting the familiar Eq. 2.4 for a Bragg grating of period Λ,

$$\lambda_B = 2n_{eff}\Lambda \tag{2.23}$$

the change in the center wavelength λ_B for a given change in grating length L, assuming isothermal conditions and neglecting higher-order terms, is given by:

$$\Delta\lambda_B = 2\left(\Lambda \frac{\partial n_{eff}}{\partial L} + n_{eff} \frac{\partial \Lambda}{\partial L} \right) \Delta L \tag{2.24}$$

Given that the path-integrated longitudinal strain is given by $\varepsilon_z = \Delta L / L$, and

$$\Delta\left[\frac{1}{\left(n_{eff}\right)^2} \right] = -\frac{2\Delta n_{eff}}{\left(n_{eff}\right)^3} \tag{2.25}$$

and assuming that

$$\frac{\partial \Lambda}{\partial L} = \frac{\Lambda}{L} \tag{2.26}$$

we can rewrite Eq. 2.24 as :

$$\Delta\lambda_B = 2\Lambda \left\{ -\frac{\left(n_{eff}\right)^3}{2} \Delta\left[\frac{1}{\left(n_{eff}\right)^2} \right] \right\} + 2n_{eff}\varepsilon_z L \frac{\partial \Lambda}{\partial L} \tag{2.27}$$

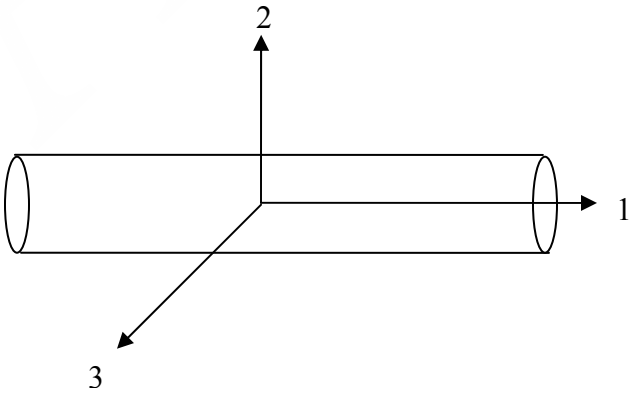

Figure 2.9 Co-ordinate axes of the optical fiber

According to strain-optic theory, the changes in the optical indicatrix tensor

$$\Delta\left[\frac{1}{\left(n_{eff}\right)^2}\right]_i$$

resulting from applied strain to the material are given by

$$\Delta\left[\frac{1}{\left(n_{eff}\right)^2}\right]_i = \Im_{ij}\varepsilon_j; i = 2,3; j = 1,2,3 \tag{2.28}$$

where ε_j is the block reduced strain tensor in the fiber and $\Im_{ij}$ is the contracted strain-optic tensor with coefficients p_{ij}, Pockel's strain-optic coefficients. The subscripts *i,j* refer to the coordinate axis as shown in Figure 2.9. For a highly-birefringent elastically isotropic fiber with the *z*- direction oriented with the 1 direction, the block-reduced strain tensor is given by:

$$\varepsilon_j = \begin{pmatrix} 1 \\ -\nu_2 \\ -\nu_3 \end{pmatrix} \varepsilon_z \tag{2.29}$$

assuming zero shear strain and ε_z being the longitudinal strain and v_i the Poisson's ratio for the fiber. The contracted ortho-optic strain-optic tensor is given by:

$$\Im_{ij} = \begin{pmatrix} p_{11} & p_{12} & p_{13} \\ p_{21} & p_{22} & p_{23} \\ p_{31} & p_{32} & p_{33} \end{pmatrix} \tag{2.30}$$

Using the results above, the longitudinal strain sensitivity can be shown to be:

$$\left(\frac{\Delta\lambda_B}{\lambda_B}\right)_i = \left(1 - p_{e_i}\right)\varepsilon_z$$

$$p_{e_i} = \frac{\left(n_{eff}\right)^2}{2}\left[p_{1i} - \nu_i\left(p_{i3} + p_{2i}\right)\right] \tag{2.31}$$

where p_{e_i} is an effective photoelastic constant (Pockel's constant). For low-birefringent optical fibers the strain optic tensor is isotropic, so that $p_{11} = p_{22} = p_{33}$, $p_{12} = p_{13} = p_{23}$ and $v_2 = v_3$, so Eq. 2.31 reduces to:

$$\left(\frac{\Delta\lambda_B}{\lambda_B}\right) = \left(1 - p_e\right)\varepsilon_z = K_e\varepsilon_z \tag{2.32}$$

where K_e is a characteristic strain constant.

Following a similar intuitive approach, the amount of wavelength shift under both transverse and longitudinal strain can be expressed as [13]:

$$\left(\frac{\Delta\lambda_B}{\lambda_B}\right) = \varepsilon_l - \frac{n_{eff}^{\ 2}}{2}\left[p_{11}\varepsilon_t + p_{12}\left(\varepsilon_l + \varepsilon_t\right)\right] = K_l\varepsilon_l + K_t\varepsilon_t \tag{2.33}$$

where ε_t, K_t and ε_l, K_l are the transverse and longitudinal strains and constants respectively.

For a typical low-birefringent optical fiber, $p_{11} = 0.17$, $p_{12} = 0.36$, $\nu = 0.16$ and $K_l = 0.78*10^{-6}/\mu\varepsilon$ and $K_t = -0.387*10^{-6}/\mu\varepsilon$. ($\varepsilon_z$ is typically expressed in microstrains $\mu\varepsilon$) [13,26].

2.4.2 Temperature sensitivity

The thermal response of fiber gratings results from the inherent expansion of the fiber material, leading to a fractional change of the grating pitch, and the temperature dependent refractive index of the fiber. The temperature sensitivity of a bare fiber is primarily due to the thermooptic effect and is expressed by [15]:

$$\left(\frac{\Delta\lambda_B}{\lambda_B}\right) = \left\{\alpha_f + \frac{1}{n_{eff}}\frac{dn_{eff}}{dT}\right\}\Delta T$$

$$= K_T \Delta T \tag{2.34}$$

where α_f is the coefficient of thermal expansion(CTE) of the fiber and K_T is the temperature coefficient.

Chapter 3: Determination of Round Exit Velocity

3.1 Introduction

The main objective of this research was to develop a system to accurately measure the Round Exit Velocity (REV) of a projectile weapon in medium and large artillery systems. The study of the interior ballistics of an artillery system (Figure 3.1) shows that when a projectile passes along a gun barrel, it is accelerated to a high velocity by the burning of propellant. The propellant may travel with the projectile or be stationary in the barrel. The gases produced by the burning propellant are trapped in the volume behind the projectile. The introduction of more heat into the product gases causes the pressure to rise, which in turn accelerates the projectile, until it exits at the muzzle. Our interest is to precisely compute the exit velocity (REV) of the projectile.

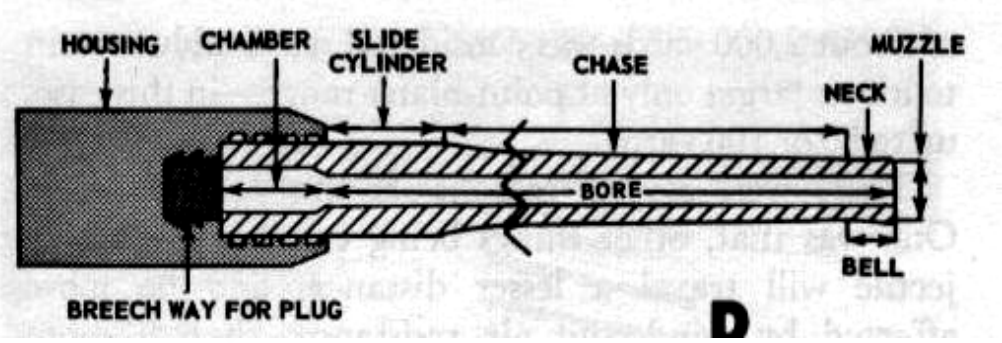

Figure 3.1 Cross-section of a M242 gun barrel deployed in the military arsenal.

The capability to monitor the Round Exit Velocity (REV) real-time and in-field can greatly improve health monitoring and enhance performance of an artillery system [22, 30]. Moreover, the REV can be used for automatic fuse programming for air

burst rounds. Important measures of gun system performance include round impact accuracy and dispersion. The impact accuracy on target of a given round in modern cannons is determined by the precision in computing the azimuth and elevation coordinates by the fire control system. These coordinates are calculated by solving a set of external ballistic equations, for which the REV of the projectile is a critical input. Currently, in most fielded gun systems, the capability to directly measure the REV does not exist. It is estimated based on nominal ammunition requirements and material properties and standard operating environments. However, during actual firing environments, factors such as barrel temperature, ammunition temperature and barrel wear can affect the REV. For example, high ammunition temperature elevates the propellant burn rate resulting in 5-10% increase in pressure and REV. Barrel wear can cause a significant REV reduction to the order of 20%. Development of system that can provide an accurate estimate of the REV based on continuous statistical data drawn from current ammunition and operating conditions would improve the accuracy of the external ballistic solution and offer a better estimate of the REV. This would directly enhance the target accuracy. Further, data from a real-time REV monitor can be used as a metric for barrel wear and tear and barrel lifetime. This would improve upon present methods which keep track of the number of rounds fired from a given barrel to determine the lifetime. Finally, the REV system can be incorporated into a real-time automatic fuse programming system for air-burst munitions on automatic medium caliber guns such as the M242 gun system. In such a system, a fuse setting system can be used to communicate time-to-destruct

information to a timer-based fused munition soon after it exits the muzzle. This can be used for automatic fuse programming for every round in a burst.

The purpose of this research was to develop a system to determine the Round Exit Velocity of a projectile while it is still in-bore, using surface mounted fiber Bragg grating sensors (FBGs). Highly pressurized propellant gases accelerate the projectile down the bore of the barrel which generates a moving hoop strain wave in its wake. This hoop strain can be detected using surface mounted FBGs near the muzzle. The center wavelength of FBGs shifts linearly in response to axial and radial strains. The velocity can thus be determined by timing the passage between two fixed points on the muzzle.

The previous chapter examined the fundamental characteristics of FBGs. In this chapter, we will review the various methods currently employed to measure REV, illustrating their disadvantages while being deployed in a field system.

3.2 Current Techniques for REV Measurement

There are a number of techniques currently employed to measure REV in field and laboratory environments. Field systems typically employ an external device (e.g. antenna array) to measure the REV after the round exits the muzzle. For laboratory environments, yaw screens, pressure transducers or strain gages are typically mounted for REV measurements [22, 30].

3.2.1 Radar based systems

For REV measurements in actual firing environments, muzzle velocity radars are employed on some field artillery systems. The M94 Muzzle Velocity Radar (MVR)

system, currently fielded by the U.S. Marines, employs a flat phased array antenna typically mounted onto the non-recoiling structure of a Howitzer gun system. This system directly measures the velocity of the outgoing projectile via Doppler shift. The Doppler shift is given by:

$$f_d = -\frac{2v}{c} f_c \cos(\theta) \tag{3.1}$$

where v is the relative velocity, f_d is the change in frequency, f_c is the frequency of the transmitted waves, θ is the angle between the source and the direction of motion and c is the velocity of light. The MVR system uses a flat antenna array to transmit the RF signal and a patch antenna for linear polarization, a radio frequency module and a data acquisition and signal processing module which performs filtering. The MVR can detect velocities in the range 50-2000 m/s with 0.1% accuracy [31].

3.2.2 Surface mounted sensor systems

For laboratory environments, yaw screens, inductive timing rings, pressure transducers and strain gages are often employed for measurement of REV. Yaw screens and inductive rings are similar in application in that they are used to measure the passage of a projectile through two inductive coils. Typically, the coils are mounted a short distance away from the muzzle and measure REV by timing the passage of the projectile between two screens (or rings). Knowing the distance between the screens or rings and the elapsed time of travel between them, one can compute REV. Pressure transducers, installed in the barrel can detect the high pressure wave caused by propellant gases as they move down the barrel. The

transducers are spaced nominally on the muzzle. The REV is calculated similar to the timing ring method. Foil strain gages are also often used to detect the passage of hoop strain which is caused by the accelerating projectile. Again, the REV is calculated as previously.

3.3 Analysis of REV Measurement schemes

The previously mentioned REV measurement techniques present tough challenges and inherent drawbacks for deployment on a field armament. Radar based systems, like the MVR are complex, bulky and expensive. It also emits active radar pulses which maybe harmful. More importantly, the operational principle of the radar based systems is based on the measurement of REV while the projectile is in flight and already target-locked [22, 30]. Hence it cannot be incorporated into the automated fuse setting system for fuse timing of that round.

The placement and installation of yaw screens and timing rings is a hindrance for easy application in a field environment. They need to be mounted by means of an external structure, which could obstruct the projectile path. Further, shock and vibration effects and high temperatures and pressures in the muzzle, demand that the structure be heavy and sturdy. The addition of significant mass at the end of the gun barrel adversely affects the gun barrel flexure dynamics leading to an increase in flexure induced aiming errors and limits the performance of the gun stabilization system.

Pressure transducers need to be barrel-mounted and require drilling holes on the surface of the barrel. This creates safety and reliability issues while deployed in field systems.

The use of electrical-resistance strain gages for ballistic research dates as far back as the early 1940's. However, they have significant drawbacks in this application, such as: slow data capture rates of measurement instrumentation, non-automated measurement techniques and sensor error due to electromagnetic interference (EMI).

3.4 Fiber optic sensors for REV measurement

Optical fiber sensors offer obvious advantages in comparison the REV measurement techniques outlined above. Optical fibers are lightweight and compact. They are mechanically robust and can operate in environments producing high shock and vibrations as well as extremes of temperature. The mechanical strength of the optical fiber has been measured to be 5-7 GPa, which is about 7 to 10 times that of carbon steel.

The use of optical fibers has been reported in applications spanning wide temperature ranges from cryogenic (-270˚C) up to nearly 1000˚C [30]. Their small size and geometric compatibility with composite materials allow them to be relatively nonperturbative when embedded, which allows *in situ* monitoring of strains within composite laminates. This has been one of the driving factors behind the adoption of fiber optic sensors in smart structure applications. Further, fiber sensors offer electrical passivity, high sensitivity and multiplexing capabilities. Finally, optical signals are immune to electromagnetic interference inherent in explosive environments. This obviates the need for extensive shielded connections required for electrical strain gages in electromagnetically noise environments.

There are two candidate technologies for forming the sensing elements which would satisfy the specifications of this application, namely in-fiber Fabry–Perot (IFFP) etalons and fiber Bragg gratings (FBGs)[20]. Both technologies rely upon forming a localized sensing region in a length of optical fiber. However, the modes of operation and the complexities of their fabrication differ considerably. An IFFP etalon is formed between two reflective surfaces, either between a semi-reflective splice and a mirrored fiber end or between the cleaved ends of two optical fibers. The change in phase of the interferometer can be used to detect the onset of the passing hoop strain. However, the complexity of their fabrication, issues regarding the reproducibility of the fabrication process, the difficulty of multiplexing arrays of IFFP sensors and poor signal-to-noise characteristics of low-reflectivity devices, combined with the electronic complexity of conditioning the output to be compatible with data-acquisition systems used for conventional strain gauges ruled out the use of IFFP etalons for this system. On the other hand, fiber Bragg grating sensors offer significant advantages. The fabrication of FBGs is relatively simple and repetitive. They offer very large multiplexing capabilities. Multiplexed arrays of FBG sensors have been successfully demonstrated in research [31]. Finally, they can be easily incorporated into conventional high speed data acquisition systems.

In the ensuing chapters, we detail the system design and the operational principles of a FBG-based REV measurement system and provide results from live-fire tests in field environments.

Chapter 4: System Design

4.1 Introduction

The design of the optical fiber sensor based REV measurement system relies heavily on the interior ballistics of the gun barrel. The first part of the ignition chain for the projectile is the primer, which contains pressure sensitive explosive compounds that detonate the propellant when struck. The rapidly burning propellant creates very high pressures in the barrel bore causing the projectile to accelerate. As the projectile is set in motion, the propellant behind it produces important effects on the interior and exterior surfaces of the gun barrel. The particular strain phenomenon of interest is the moving hoop strain produced by the accelerating projectile as it moves along the barrel and exits at the muzzle. Measurement of this propagating hoop strain would indirectly be a measure of the projectile's exit velocity. An important side effect of this process is the accompanying temperature rise in its vicinity and causes thermal expansion of the barrel walls.

The advantages of using a fiber optic strain sensing mechanism to detect hoop strain have been clearly established. In this section, we elaborate on the operational principles of the fiber Bragg grating based REV system in view of the system design specifications, the construction of the REV measurement system and the results of laboratory and field experiments.

4.2 Operational Principles

The underlying principle of operation employs the use of fiber Bragg grating (FBG) sensors to detect strain changes. An FBG is a periodic modulation of the core refractive index of an optical fiber. FBGs operate as a wavelength selective filter for transmitted light. More interestingly, in reflection it produces a sharply peaked narrow spectrum. The center wavelength of the reflected spectrum is the Bragg wavelength λ_B which is related as (Eq. 2.4):

$$\lambda_B = 2n_{eff}\Lambda \tag{4.1}$$

The center wavelength of the FBG shifts in response to external strain or temperature effects. This is due to changes in the refractive index (n_{eff}) due to temperature or strain as well physical elongation to the fiber causing a variation in the grating period Λ. The effect of strain and temperature can be treated independently of one another and the overall FBG response can be characterized by studying the response of the FBG to strain and temperature individually and then summing up the two effects. Combining the effects of temperature and strain from Eq. 2.32 and 2.34:

$$\left(\frac{\Delta\lambda_B}{\lambda_B}\right) = \left(1 - p_e\right)\varepsilon_z + \left\{\alpha_f + \frac{1}{n_{eff}}\frac{dn_{eff}}{dT}\right\}\Delta T \tag{4.2}$$

where the symbols have their usual meanings.

However, in the case of the sensor bonded to a structure (e.g. gun barrel), the effects are modified slightly.

This is because we need to consider various other effects: expansion of the structural material, strain transfer from the barrel wall to the FBG sensor and bonding of the epoxy adhesive which attaches the FBG to the barrel. In this case Eq. 4.2 is modified as [25]:

$$\left(\frac{\Delta\lambda_B}{\lambda_B}\right) = \left(1 - p_e\right)\varepsilon_z + \left\{p_e(\alpha_s - \alpha_f) + \zeta\right\}\Delta T \tag{4.3}$$

where α_s and α_f are the coefficients of thermal expansion of the barrel material and the fiber respectively, p_e is the Pockel's coefficient of the strain-optic tensor and ζ is the thermo-optic coefficient.

The linear variation of the center wavelength shift of the bonded FBG in response to temperature and strain effects are verified by the results of experiments performed as shown in Figures 4.1 and 4.2. From the results from several experiments, we can determine the following approximate values for temperature and wavelength sensitivities at 1550 nm:

Parameter	Center Wavelength shift
Temperature	.027 nm/˚C
Strain	0.0013 nm/με

Table 4.1 Temperature and strain sensitivities for bonded grating sensor

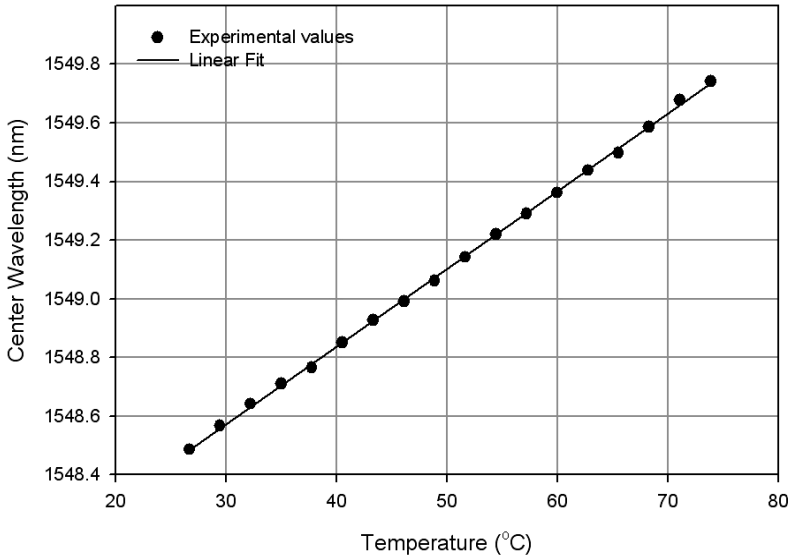

Figure 4.1 Center wavelength shift of FBG in response to temperature

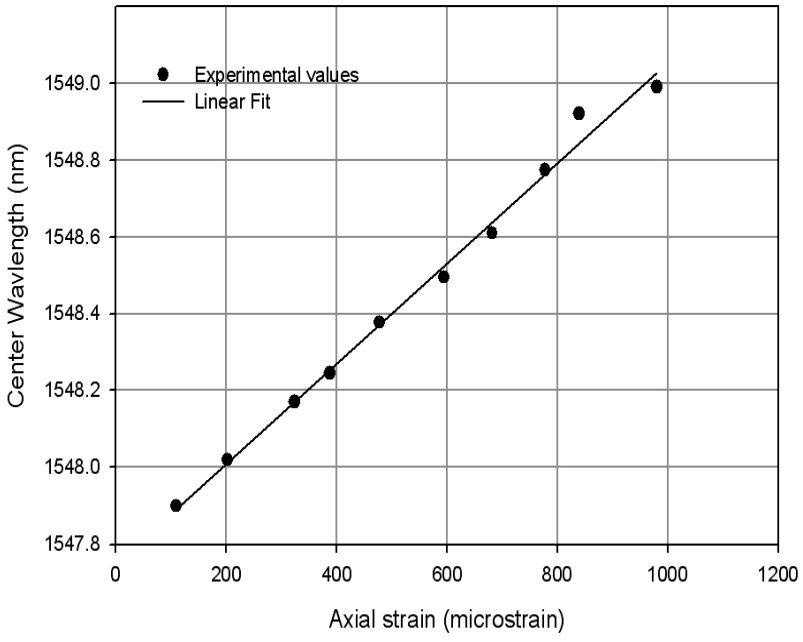

Figure 4.2 Center wavelength shift of FBG in response to strain

It is important to note that the system response is characterized only by monitoring the shift in Bragg wavelength (λ_B). Therefore only the overall strain effect is taken into account; isolation of strain into axial and radial components is not important.

The Round Exit Velocity is computed by timing the hoop strain dilation as it passes a known separation distance between the FBGs. It has been experimentally determined in live fire tests that the velocity of the projectile is relatively constant in a short section just before it leaves the muzzle [22, 30]. A correction factor for the small acceleration experienced by the projectile in the short distance between the muzzle and the unvented portion of the muzzle brake can be added to the computed REV based on empirical live-fire test results. The wavelength shift enables detection of the moving projectile as it reaches the sensor. By positioning the sensors a fixed distance L_d apart near the muzzle, and measuring the time difference Δt, of the onset of the shift in λ_B, the REV can be estimated as:

$$v_{REV} = L_d / \Delta t \tag{4.4}$$

4.3 Design specifications

The REV measurement system designed, incorporated functionality based on several design parameters as dictated by the field armament system on which it was to be deployed. The following are some important specifications [22, 30]:

- The target weapon system under evaluation was the M242 25mm cannon
- The maximum projectile velocity attained in this system is 1400 m/s.
- It was desired to achieve a velocity measurement resolution of < 1% of the maximum projectile velocity (i.e. 14 m/s).
- The system required ruggedization to withstand shock and vibration effects associated with field firings especially in burst mode operation.
- Further, adequate temperature compensation to achieve an operating range from 0˚C – 500˚C was desired.
- Efficient signal processing to calculate the round exit velocity of the projectile while it is still in-bore.

In order to optimize and evaluate the system design, it is necessary to understand the ballistics of projectile motion and the strain produced in the process. These can be obtained from field firing data and ballistic model predictions. Barrel strain and temperature data collected from live-fire tests show maximum strain levels of 600-1000με with strain rates as high as 500με/μs [20]. Hence, to satisfy the 1% velocity resolution, the strain resolution was determined to be 100με.

4.4 System Design

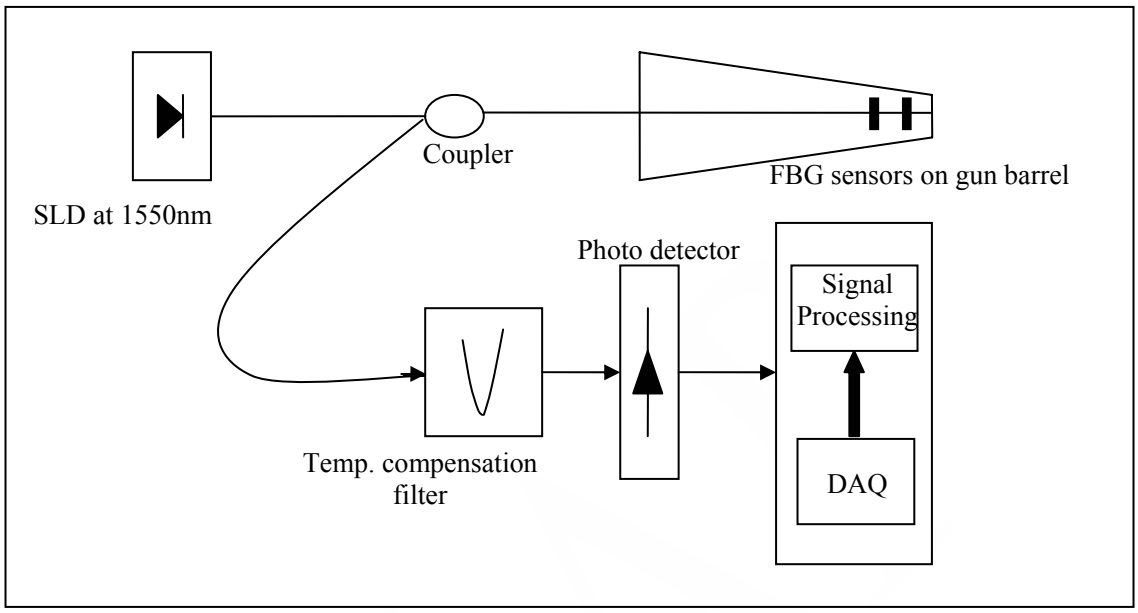

Figure 4.3 Schematic of system design for REV measurement system

Figure 4.3 above illustrates the schematic of the system design used in the REV measurement system. A broadband superluminescent diode (SLD) at 1550 nm with a FWHM of 45nm is used to illuminate the FBGs attached to the barrel, via an optical coupler. The optical coupler is in fact an optical splitter box, which splits the source signal into two components each going to the one of the sensors. The power intensity of the individual sensor input signals is one half of the SLD power intensity, the coupler introducing a 3dB loss. The light is reflected back from the FBG and transmitted over the same fiber back into the splitter. The reflected signal from each FBG is then further separated into two components by means of another 3dB coupler. One of these is sent to an optical notch filter, whereas the other serves as a power

reference signal. The output of the spectral filter is fed into an optoelectronic circuit, which consists of a photodetector and accompanying amplification circuitry. Finally, a high speed data acquisition system captures the data from the analog outputs of the optoelectronic board, which after adequate signal processing can be used to compute the round exit velocity. The following sections discuss the operation of the various components of the REV measurement system.

4.4.1 Sensor positioning

The position of the FBG sensors on the gun barrel is of critical importance for the detection of the onset of the hoop strain. As previously illustrated, the projectile velocity attains an almost constant velocity near the muzzle. The minute acceleration it experiences can be factored in based on statistical system data. The Bragg gratings are epoxied in place circumferentially on the barrel surface and perpendicular to the barrel axis. In this position, they are most sensitive to the propagating hoop strain wave. In order to achieve the velocity accuracy and system resolution goals, the nominal sensor spacing was determined to be around 10 -15 cm. However, the geometry of the barrel system also needs to be considered. The material thickness near the muzzle varies slightly due to the tapered profile of the barrel. In some systems, the bore may have a step profile, with each step having a different thickness. A greater thickness implies more thermal mass. This may affect the strain transfer from the barrel onto the sensors. The different sections may also expand at different thermal rates. Therefore, to arrive at an optimal spacing configuration, several sensors

were arranged at different spatial intervals. Figure 4.4 shows multiple FBG sensors attached to a gun barrel system.

Figure 4.4 Fiber Bragg grating sensors mounted on a gun barrel system

From Eq. 4.4 we can calculate the minimum time resolution, $d\Delta t$, required for the sensing system to measure the REV to within the required resolution dv_{REV}/v_{REV} as:

$$d\Delta t = (L_d / v_{REV}) \frac{dv_{REV}}{v_{REV}} \tag{4.5}$$

Assuming the spacing L_d = 0.25m, v_{REV} = 1400m/s and dv_{REV} = 7.8 m/s, the minimum time resolution is ≈ 1μs. This translates to a sensor bandwidth of 1 MHz. So it is clear that the detecting system and the accompanying electronics require high speed data acquisition rather than high accuracy. In other words, the sensing mechanism must accurately detect the shift in λ_B but does not necessarily have to measure the amount of shift. In order to achieve this requirement, a detection method based on an optical

notch filter was developed. The working principle of this filter is described in detail in a later section.

4.4.2 Sensor attachment

The attachment of the fiber Bragg grating sensors onto the gun barrel directly affects the detection of the hoop strain wave by the sensor. The important qualities which determine the effectiveness of a particular adhesive bonding are:

- Withstand high temperatures (up to 500˚C)
- Ability to sustain high expansion i.e. high coefficient of thermal expansion (CTE)
- Maximize Strain transfer (from barrel to the FBG).
- Ability to withstand shock and vibration effects.

There are several commercially available adhesives used in fiber optic applications, which can be classified into single or two-component epoxies, ceramic cements, polyimide-based adhesives and resins. Several adhesives were investigated for their bonding capabilities, ease of application, curing cycles and cost-effectiveness. Upon conclusion of the study, two particular adhesives, AngstromBond and M-Bond 450 adhesives were chosen for the application.

4.4.3 Light source characteristics

The broadband light source used is a superluminescent diode (SLD) at 1550 nm with a FWHM of 45nm. The source intensity is maintained via a regulated power supply. The light is transmitted through a pigtailed fiber egress to be transferred onto the barrel mounted sensors. The power intensity profile is relatively constant and fluctuates minutely due to ambient temperature changes and noise effects. Figure 4.5 shows the spectral characteristics of the superluminescent diode light source.

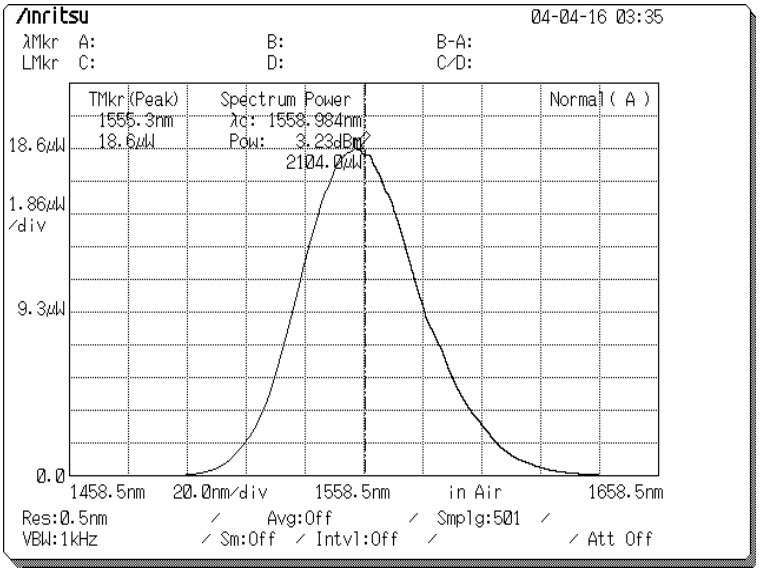

Figure 4.5 Power spectrum of the superluminescent diode

4.4.4 Spectral notch filter

A critical aspect of the hoop strain detection system is the development of a fixed filter tuned to the reflection spectrum of the sensor. The optical filter is also a fiber Bragg grating similar to our sensor gratings. However, it has a significantly larger bandwidth (i.e. FWHM) than short period gratings. While short period grating sensors have an FWHM of 0.1-0.3 nm, the filter gratings have a FWHM of 0.9 – 1.0nm.

Further, for filter spectra, we are more interested in the transmission spectrum rather than in reflection. The filter has a precisely defined optical spectrum as shown in Figure 4.6.

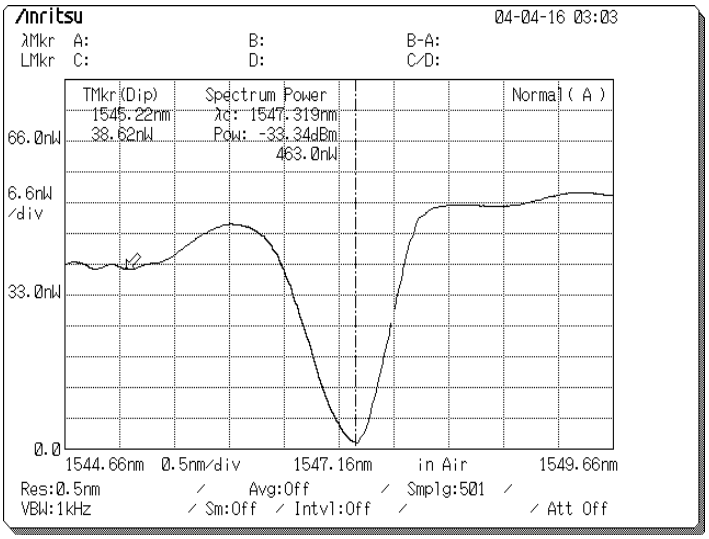

Figure 4.6 Optical intensity spectrum of the notch filter in transmission

As expected the transmission spectrum is converse to the reflection spectrum, with "holes" (no light passage) in place of the Bragg wavelength peaks.

The filter is initially tuned precisely to the FBG sensor reflection spectrum. Since, the filter has a greater bandwidth, the sensor can be placed comfortably in the spread of the filter. Figures 4.7 and 4.8 illustrate the tuning mechanism.

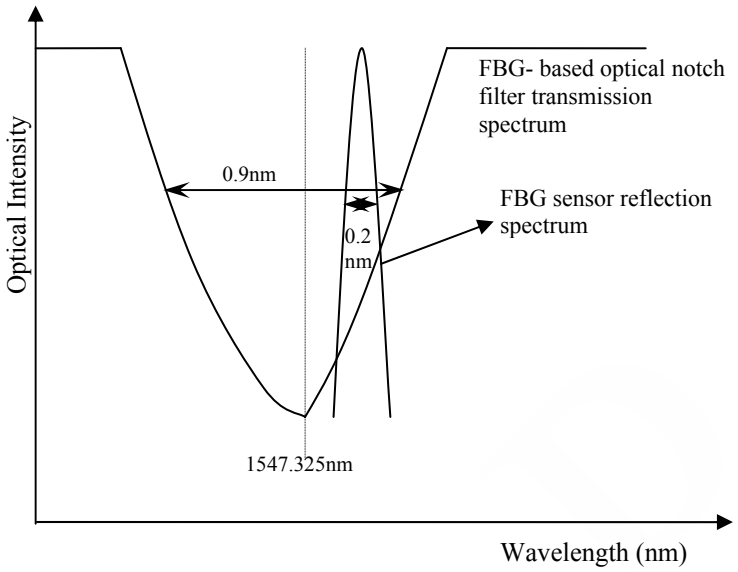

Figure 4.7 Optical intensity spectra for FBGs and notch filter in the unstrained condition

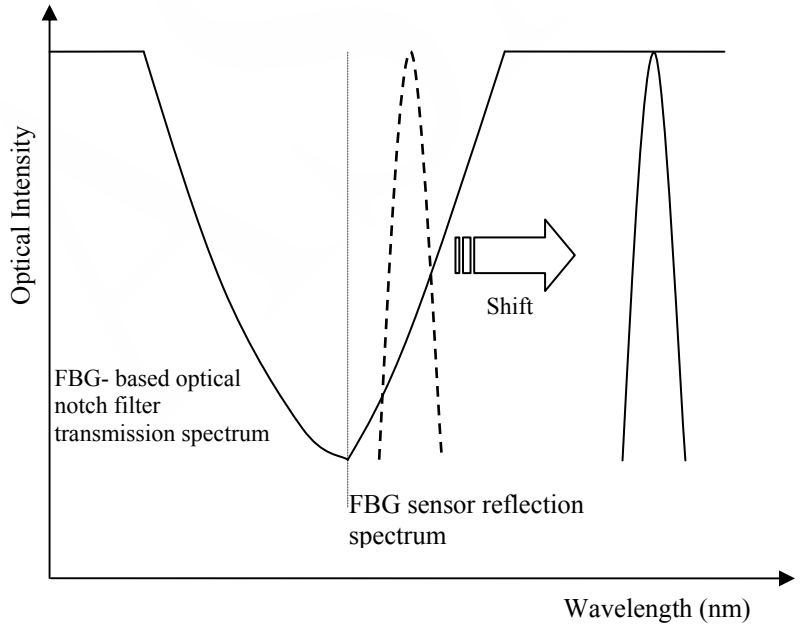

Figure 4.8 Optical intensity spectra for FBGs and notch filter in the strained condition

In the initial case, both the barrel-mounted grating sensors experience no strain. Light from the SLD is coupled through to the sensors, which reflect back a portion of the incident light. The intensity spectrum of one of the sensors is shown in Figure 4.7. The light then passes through to the notch filter and then on to the photodetector circuit, which outputs an electrical voltage linearly proportional to the input optical power. In Figure 4.7, the optical filter has been tuned to the sensor reflectance, such that the spatial arrangement in wavelength space, completely suppresses the intensity peak of the FBG sensor. The transmission of optical power is blocked and there is no light intensity throughput to the photodetector. Hence, it remains at its quiescent level.

In the event of a firing, the moving projectile produces a hoop strain which stretches the bonded sensors on the barrel, causing a shift in λ_B. As a result, the reflection peak shifts towards the longer wavelength side, and outside the notch filter "cavity". There is a throughput of light onto the photodetector. This is illustrated in Figure 4.8. The slope of the intensity spectra is sharp enough so that a small shift in λ_B can cause a significant change in the light intensity reaching the photodetector, which experiences a step-up in the input optical power. The exact situation is replicated when the hoop strain reaches the second sensor (closest to the muzzle) and as a result the second photodetector experiences a sharp step in light intensity. The separation in time between the step-ups in photodetector current is used to estimate the REV.

An accompanying side-effect of the firing events is a rise in temperature due to barrel heating. This is particularly important in continuous or burst firing modes, wherein the center wavelength not only shifts as a result of dilating hoop strain but also due to

temperature. These phenomena fortunately occur in different temporal scales. Barrel heating is one the order of minutes, while the strain pulses are on the order of microseconds. A typical time evolution of the temperature and strain events is shown in Figure 4.9.

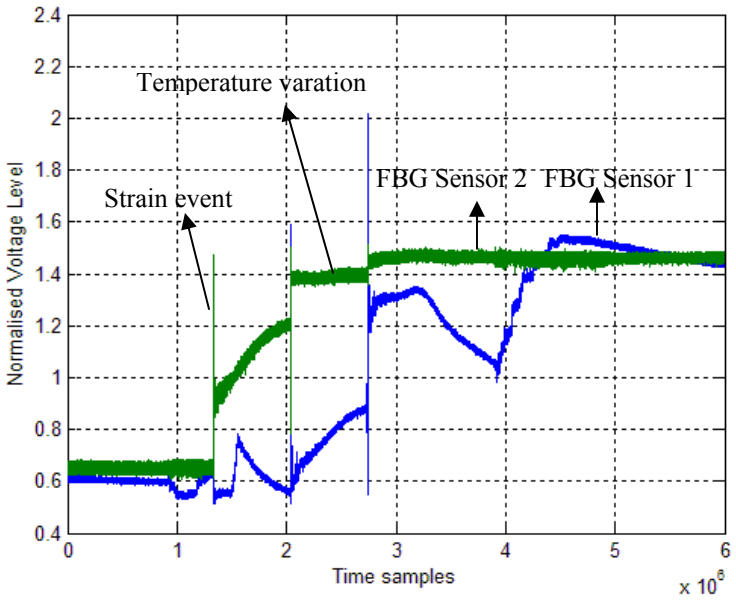

Figure 4.9 Strain and temperature variation on a temporal scale in burst mode firing

Due to the additional temperature rise, the FBG sensors do not return to their initial position (as shown in Figure 4.7) after the strain event, but remain slightly shifted due to the increase in ambient temperature. Therefore, the notch filter has to be re-tuned to line-up with the shifted reflection spectrum. A bending bar mechanism has been developed to provide adequate temperature compensation. The notch filter gratings are bonded onto steel plates which can be bent using a rotational screw mounted on a stepper motor shaft. Figure 4.10 shows the bending bar mechanism.

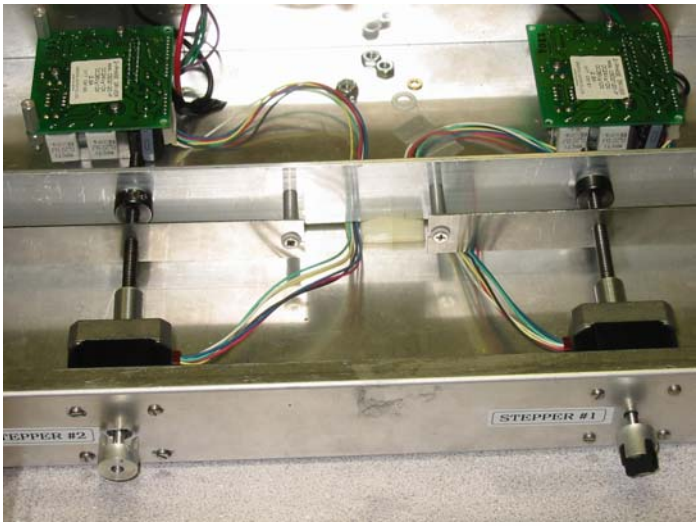

Figure 4.10 Bending bar mechanism with mounted notch filters

The flexure in the bending beams causes an elongation of the gratings leading to a wavelength shift and consequently, the transmission spectrum can be shifted and repositioned to match up to the sensor. A software interface has been designed to automate the repositioning so as to provide instantaneous temperature compensation. The wavelength range of this system is approximately 10nm which can compensate for a 370˚C rise in temperature.

4.4.5 Photodetector and Amplifier

The optical signal from the spectral filter needs to be converted to a suitable electrical form for signal processing. The optoelectronic component consists of the following elements: photodetector, amplification stages and demodulation circuits. The photodetector generates a small photocurrent in response to the intensity of incident illumination. Important metrics of photodiode performance include responsivity (ratio of electrical output to optical input), dark current (quiescent electrical output that

serves as a measure of inherent electrical system noise), speed and bandwidth. For this research, a high speed InGaAs PIN Photodiode with a responsivity of 0.95 A/W at 1550nm and bandwidth of 3.5 GHz was used. The amplification stages convert the electrical current into a voltage and subsequently boost the signal voltage for compatibility with data acquisition systems. In this project, the signal intensity at the photodiode consists of a DC signal of ~400nW with an AC signal of 200nW peak-to-peak amplitude. A two-stage amplifier has been developed consisting of a preamplifier stage and a secondary amplifier stage. The preamplifier is a low-noise transimpedance FET amplifier with high unity-gain bandwidth product and low input capacitance. We use the AD823 AN 16 MHz, 1.8pF FET amplifier for this stage. The signal from this stage is fed into a secondary stage consisting of a non-inverting operational amplifier with a gain A_v = 121. The voltage is boosted up to 1.3V at this stage. We use the CLC425 operational amplifier as it offers a high bandwidth of 1.7GHz with low input noise characteristics. Figure 4.11 shows a schematic of the amplification stages. D1 represents the photodiode, U1 is the AD823 FET amplifier and U2 represents the CLC 425 op-amp. R2 is a series resistor used to cancel bias current errors. R4 and R5 are determined from the gain equations.

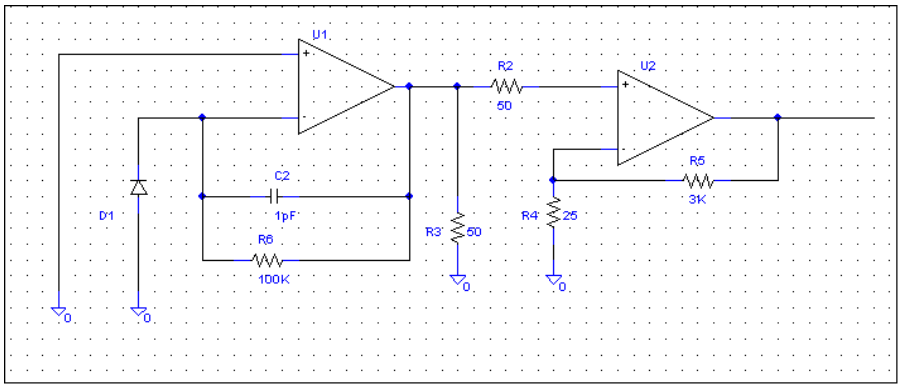

Figure 4.11 Schematic of Photodetector and amplification stages circuit

4.4.6 Signal Processing

The voltage data was collected from the optoelectronic system by means of a NI-DAQ card into a PC for signal processing. The data was sampled at 1 MHz for time durations up to 8 seconds. A typical strain response curve generated is shown in Figure 4.12. The typical rise time was found to be ~10μs with peak strain levels measured around 10000με [20].

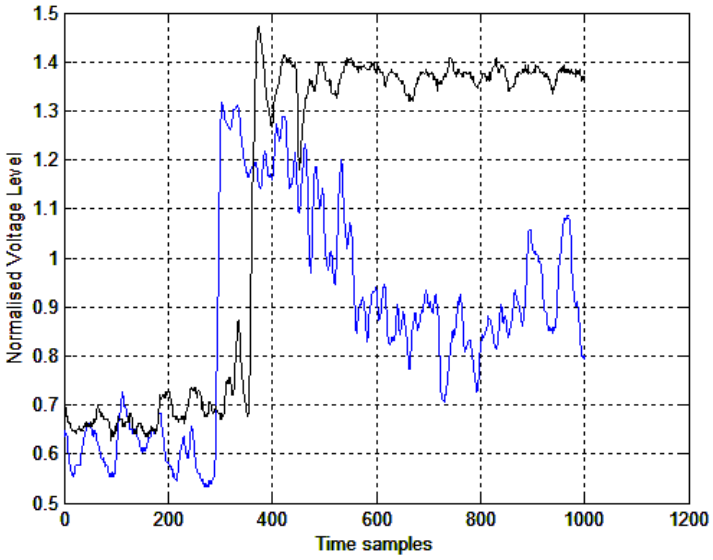

Figure 4.12 Strain response curve in single shot mode

In order to accurately determine the REV, it is important to compute the time interval between the onset of the hoop strain wave at the two fiber Bragg grating sensors. Initial estimates of round-exit velocity were obtained from simple offline visual inspection of the rise-time of the strain curves and peak detection and thresholding techniques. However, these proved to be inaccurate and non-repetitive. Moreover, in air burst mechanisms, the requirement is for a real-time velocity calculation system to measure the velocity while the projectile is still in-bore. Since the fuse setting

mechanism is only a short distance away from the sensing system, the loop time for velocity calculation must be under 60μs.

An improved approach based on short-time Fourier analysis and cross-correlation of the two response curves has been developed. A Fourier analysis of the signal shows that the significant portion of the strain response curve has frequency content in the range 20-200 KHz. Figure 4.13 depicts the frequency spectrum of continuous mode firing event whose strain response was shown in Figure 4.9

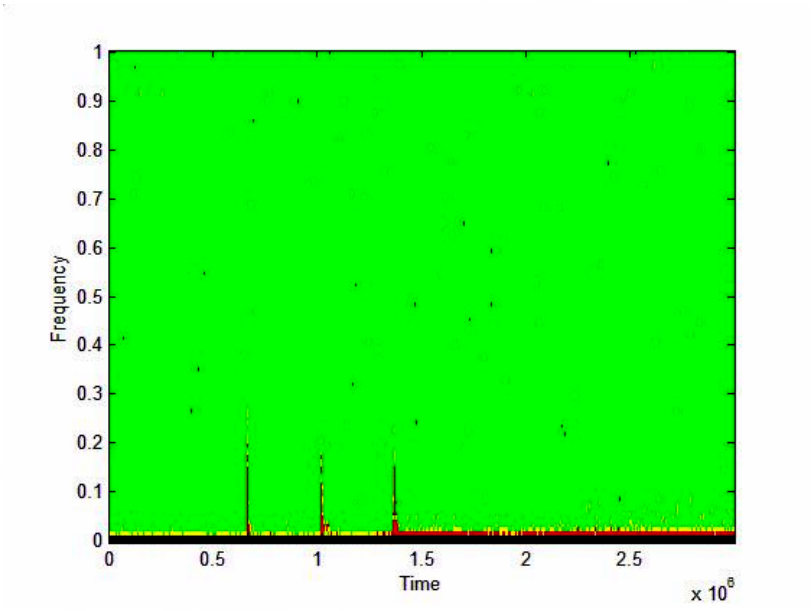

Figure 4.13 Frequency content of strain wave in continuous mode firing

The temporal variation of temperature is on a much slower time scale and appears as a DC shift in the frequency spectrum. Higher frequencies (> 250 KHz) are due to acoustic ringing phenomena as a result of sound vibrations associated with the moving projectile. As such these frequencies can be low-pass filtered. Also, to remove noise components introduced to the system components, thresholding is performed to retain the signal above the noise floor. Additionally, smoothing filters

are applied to remove unnecessary spikes which may lead to distortion effects. The timing information is then extracted by computing the cross-correlation between the signals produced by the FBGs. Figure 4.14 shows the cross-correlation function for a single strain event detected by both the FBG sensors.

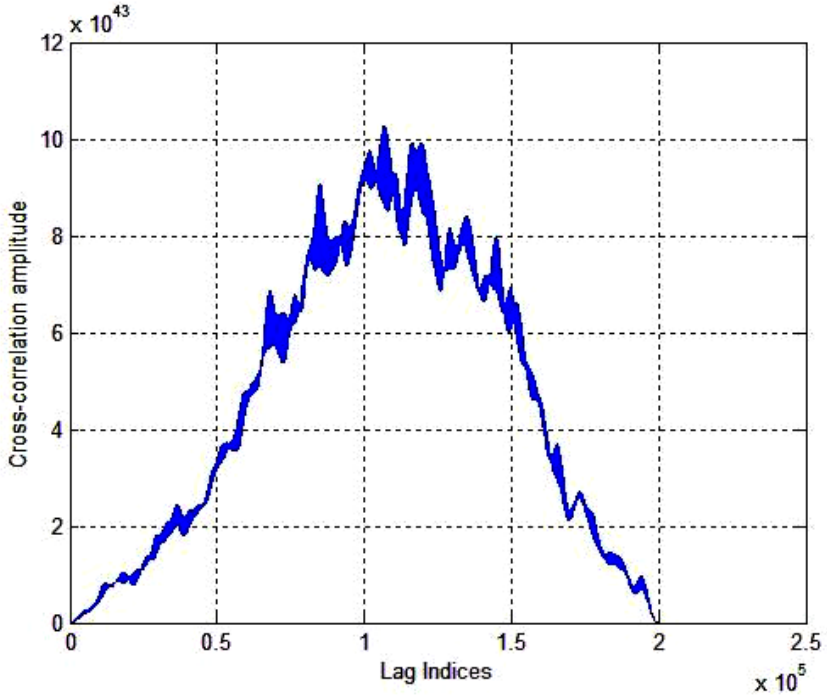

Figure 4.14 Cross-correlation spectrum for a single firing event

The maximum cross-correlation is a measure of the signal amplitude corresponding to the event of maximum strain transfer i.e. the exact instance when the projectile causes the circumferential expansion of the barrel near the FBG sensors. The time lag at the point of maximum cross-correlation is an estimate of the elapsed time between the strain events at the two FBGs separated by a short distance. Knowing the distance, we can accurately estimate the exit velocity of the round as it leaves the muzzle. This methodology allows for real-time, efficient and accurate measurement of the REV,

provided the data sampling rates are high and the signal processing can be performed on a fast, and dedicated processor. REV estimates from live fire data validate the use of the cross-correlation algorithm, as shown in the following section.

4.5 Results

Live fire tests were conducted on two M242 gun barrel systems at the US Army arsenal. The FBG sensors were attached within 4.5 cm of the muzzle and spaced approximately 10 cm apart. Data was collected through a NI-DAQ system through a LabView interface. A Weibel Scientific W-680I Doppler Analyzer was used a reference system to determine the muzzle velocity based on its trajectory. The system is limited by measurement of the muzzle velocity of the first round in a multiple round burst. Several tests for varying ammunition types and single and burst shot modes were performed. Data was collected from the FBG sensors, optical reference channels and the Weibel radar system at varying sample rates from 800 Hz -2 MHz. The data was post-processed and the REV was computed using the cross-correlation algorithm. The maximum temperature achieved in the firings was 200˚C, which is way below the design specifications. Table 4.2 shows representative data from the live fire tests.

			Bragg grating sensor velocity calcn.		
Test #	Shot #	Weibel velocity	Visual inspection	Correlation Algo	% Error
2	1	1490	1502	1494	0.268456
9	2	1485	1545	1466	-1.27946
11	2	1481	1523	1524	2.903444
11	3	1479	1460	1471	-0.54091
12	2	1486	1401	1396	-6.05653
12	3	1485	1501	1550	4.377104
12	4	1485	1557	1471	-0.94276
13	1	1492	1401	1432	-4.02145
13	2	1493	1460	1530	2.478232
15	3	1306	1335	1300	-0.45942
15	4	1316	1681	1380	4.863222
16	3	1310	1368	1324	1.068702
16	4	1318	1366	1301	-1.28983
17	1	1312	1262	1320	0.609756
17	2	1321	1401	1367	3.48221
19	1	1321	1294	1365	3.33081
21	5	1319	1278	1333	1.06141
21	6	1317	1766	1291	-1.97418
22	1	1330	1430	1275	-4.13534

Table 4.2 Results from live fire tests

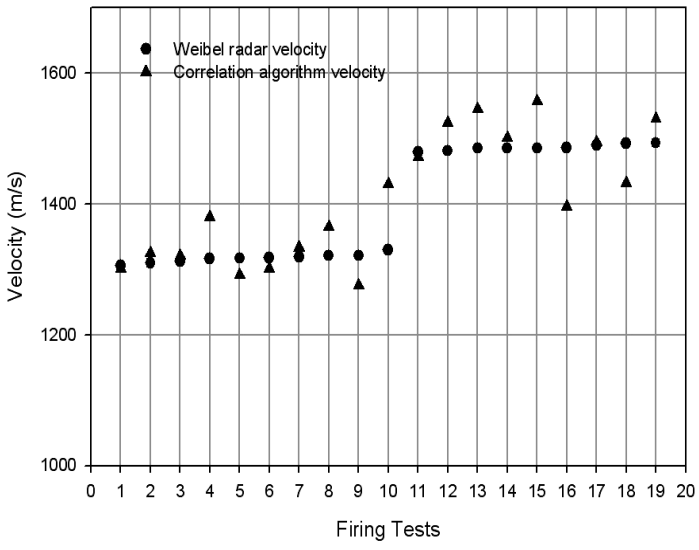

Figure 4.15 Comparison of correlation algorithm REV and radar reference

Figure 4.15 shows the comparison between the REV calculated using the correlation algorithm and the Weibel radar reference velocity. The average error was found to be 1.19 %. This compares well with the target accuracy of 1% error. The error for Test #12 and #15 was high due to inadequate temperature calibration and compensation issues. Also, the data from burst mode operations indicates that the system response is sufficiently fast with adequate resolution to enable measurement of REV at firing rates up to 200 rounds per minute. Finally, the system held up well under shock and thermal loads generated during the firing tests and there was no evidence of failure of bonding mechanisms or temperature-related degradation.

Chapter 5: Conclusions and Future Work

In this thesis, a fiber Bragg grating sensor based system for measuring round exit velocity of a projectile in medium caliber gun systems has been designed, fabricated and tested. The live-fire results show that the proposed method can accurately measure the REV to within 1-2% error as compared to external methods of detection. The system also demonstrated considerable robustness to withstand the high shock and thermal loads generated in firing tests. The cross-correlation algorithm provides an accurate estimate of the REV with the capability of incorporation into automated real-time signal processing modules. This sensor system will provide invaluable velocity information that can be used in structural health monitoring of field-deployed armament systems, to enhance gun system performance and improve the target accuracy when incorporated into an automated fuse programming control system. The current scheme requires further research on automated filter scanning and signal processing. This is necessary due to the large shifts in the Bragg wavelength caused by heating of the gun barrel in repetitive firings. In contrast to the case of a superluminescent diode (SLD), when a conventional laser diode (LD) illuminates a FBG, there is very little reflected light, unless the LD wavelength matches the Bragg wavelength closely. Consequently, if the laser diode wavelength is servoed to the Bragg wavelength in a slow servo loop, then there is negligible variation in the reflected signal on a slow time scale. If the LD is modulated at a low frequency, the servo can continuously keep adjusting the LD wavelength over several nm in response to slow temperature variations and maintain maximum reflection. The onset

of the hoop strain causes a rapid shift in center wavelength and a time scale too fast for the servo control mechanism to compensate. The resulting signal can be high pass filtered and processed for timing information. Figure 5.1 shows a schematic of the proposed mechanism.

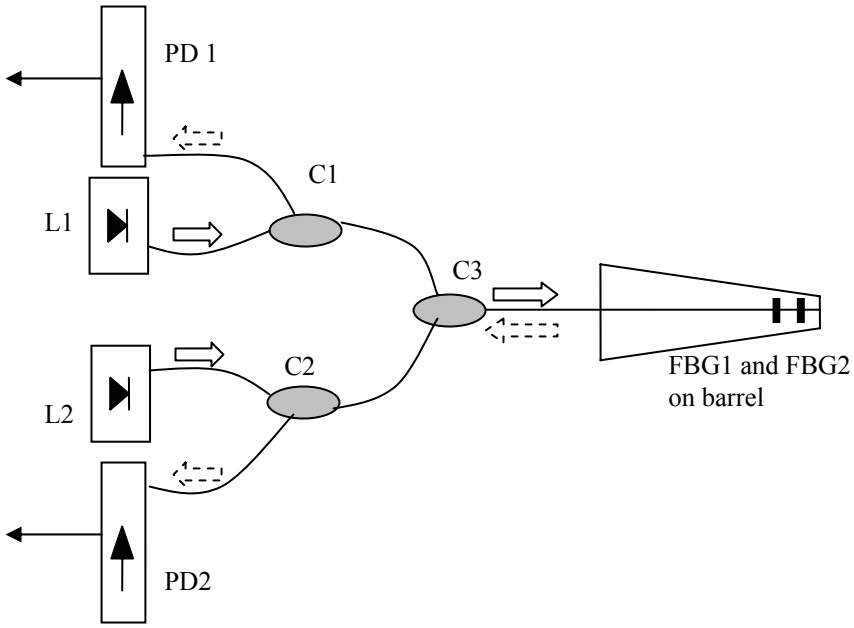

Figure 5.1 New CWDM approach to strain pulse timing

In the figure, L1 and L2 are two different wavelength lasers servoed to the FBG peaks to maintain maximum reflectivity. C1 and C2 are conventional 3 dB couplers. C3 is a coarse wavelength division multiplexing (CWDM) coupler that combines the two different laser signals over a single fiber. The reflected signals are coupled back via C3 to photodiodes PD1 and PD2 and then onto amplification circuitry and filtering mechanisms.

Additional work also has to be done to integrate the data acquisition system and the signal processing onto a dedicated DSP processor to provide real-time and accurate

velocity measurements. The future direction of this research will look at improving the current methodologies and incorporating better ideas to provide a faster and more accurate round-exit velocity measurement system.

Appendix A: Technical Data on the Experimental Setup

In this section, technical data and specifications of the various components of the REV measurement system is provided.

- **Fiber Bragg grating sensors:** Custom made FBG, wavelength: 1550 ± 0.05 nm, reflectivity: 97% ±3%, fiber: Corning SMF-28 polyimide fiber, fiber length: 1.5m, recoating: polyimide, grating length: < 30mm.
- **Source:** Superlum Diode SLD-761 superluminescent diode at 1550 nm with FWHM 45nm, attached to pigtailed fiber.
- **Optical Spectrum Analyser:** Anritsu MS9710 OSA, resolution: 70pm, wavelength accuracy: ± 50 pm when calibrated
- **Couplers:** Newport optical 3dB single mode fused coupler at 1550nm.
- **Broadband optical Notch filter**: Custom made FBG, wavelength: 1547 ± 0.05 nm, bandwidth: 0.9 ± 0.01nm, reflectivity: 99% ±1%, fiber, recoating: polyimide, grating length: < 30mm.
- **Filter mechanism:** Bending beams: Custom machined stainless steel plates 20cm x 5cm x 0.5 cm. mechanically bent using stepper motor controller and driver.
- **Detector**: High speed InGaAs PIN Photodiode, responsivity: 0.95 A/W @ 1550nm, operating voltage: 5V, bandwidth: 3.5 GHz, rise and fall time: 0.07 ns.
- **Amplification stages**: AD 823 AN FET amplifier, unity-gain bandwidth product: 16MHz, input capacitance 1.8pF, input bias current: 3pA.

Appendix B: Code Segments

B.1 MATLAB cross-correlation algorithm

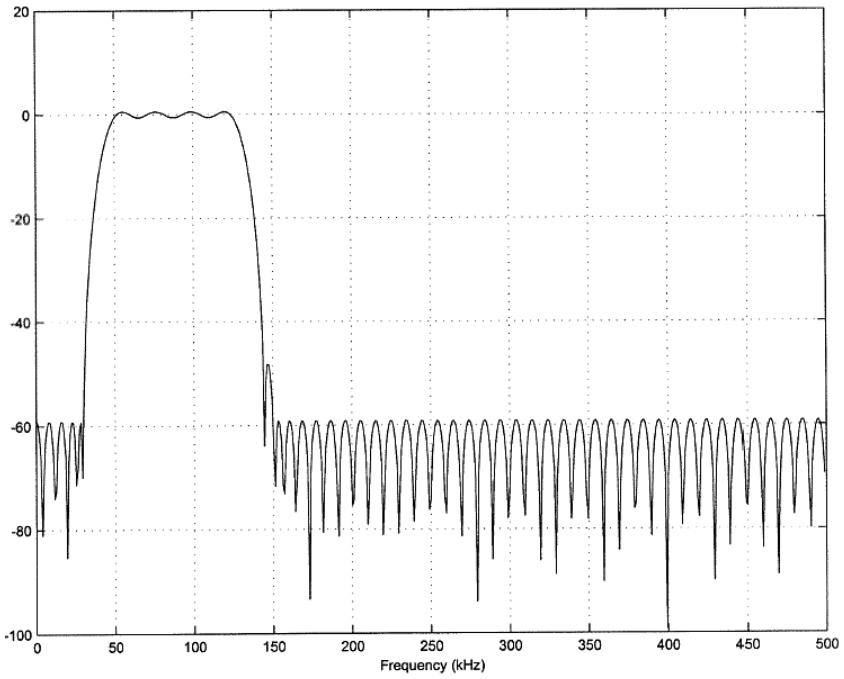

Figure B.1 Filter profile for signal processing

B.1.1 MATLAB code segment for Cross-Correlation

```
cd shots
dir
load shot3
load fil
ch1fil=filtfilt(b,1,shot3(:,1));
ch2fil=filtfilt(b,1,shot3(:,2));
[y,i]=max(abs(interp(ch1fil,100)),abs(interp(ch2fil,100))
)
[y,i]=max(xcorr(abs(interp(ch1fil,100)),abs(interp(ch2fil
,1,100))
plot(downsample(shot3(:,1),5))
```

B.2 MATLAB code segment for filter operation

```
ai = analoginput('nidaq',1);
chan0=addchannel(ai,0,{'chan0'});
chan1=addchannel(ai,1,{'chan1'});

ai.chan0.InputRange = [0 5];
ai.chan1.InputRange = [0 5];
set(ai,'SampleRate',1000);
set(ai,'SamplesPerTrigger',1);
set(ai,'TriggerType','Manual');
ai.InputType='NonReferencedSingleEnded';

dio = digitalio('nidaq',1);
addline(dio,0:7,'out');

s1=serial('COM1');
fopen(s1);
s1.Terminator='CR';
pval=[1 1 0 0 0 0 0 0];
putvalue(dio,pval);
fprintf(s1,'LBL testIO\n');
fprintf(s1,'Msel=250\n');
fprintf(s1,'Munit=51200/1041.4\n');
fprintf(s1,'Pos=0\n');
fprintf(s1,'Vm=1000\n');
fprintf(s1,'Ios 21=9,0,1\n');

i=1;
step_max =210; % CHANGE
while (i<step_max)
    j=0;
    avg0=0;
    avg1=0;
    while (j<30)
        start(ai);
        trigger(ai);
        ach=getdata(ai);
        ach0=ach(1);
        ach1=ach(2);
        avg0=avg0+ach0;
        avg1=avg1+ach1;
        j=j+1;
    end
    fil_1(i)=avg0/30;
    fil_2(i)=ach1/30;
```

```
    i=i+1
    pval=[1 1 0 0 0 0 0 0];
    putvalue(dio,pval);
    fprintf(s1,'movr -5\n'); % CHANGE
end

smooth1=sgolayfilt(fil_1,3,41);
smooth2=sgolayfilt(fil_2,3,41);
diff1=diff(smooth1);
diff2=diff(smooth2);
max_1=max(diff1);
max_2=max(diff2);
plot(fil_1);
save('filter1','fil_1');
pause
i=1;
while (i<200) % CHANGE
    if (diff1(i)==max_1)
        step_1=i;
    end

    if (diff2(i)==max_2)
        step_2=i;
    end
    i=i+1;
end
step_1=step_max-step_1;
step_2=step_max-step_2;
pval=[1 0 0 0 0 0 0 0];
putvalue(dio,pval);
fprintf(s1,'movr +%d\n',step_1);
start(ai);
trigger(ai);
ach=getdata(ai);
ach0=ach(1);

while (~(ach0< fil_1(step_1)))
    pval=[1 0 0 0 0 0 0 0];
    putvalue(dio,pval);
    fprintf(s1,'movr +5\n');
    j=0;
    avg0=0;
    while (j < 30)
        start(ai);
        trigger(ai);
        ach=getdata(ai);
        ach0=ach(1);
```

```
        avg0=avg0+ach0;
        j=j+1;
    end
    ach0=avg0/30;
end

pval=[0 1 0 0 0 0 0 0];
putvalue(dio,pval);
fprintf(s1,'movr +%d\n,step_2');

while (~(ach1< fil_2(step_2)))
    pval=[1 0 0 0 0 0 0 0];
    putvalue(dio,pval);
    fprintf(s1,'movr +5\n');
    j=0;
    avg1=0;
    while (j < 30)
        start(ai);
        trigger(ai);
        ach=getdata(ai);
        ach1=ach(1);
        avg1=avg1+ach1;
        j=j+1;
    end
    ach1=avg1/30;
end

fclose(s1);
delete(s1);
```

Bibliography

[1] C. C. Davis. *Lasers and Electro-Optics*. Cambridge University Press, 1996.

[2] Johannes Skaar. *Synthesis and characterization of fiber Bragg gratings.* Thesis submitted to Institute of Physical Electronics, Norwegian University of Science and Technology, Nov 2000.

[3] J. Skaar. *Synthesis of fiber Bragg gratings for use in transmission*. Journal of the Optical Society of America A, vol. 18, no. 3, pp. 557-564, March 2001.

[4] K. O. Hill, Y. Fujii, D. C. Johnsen, and B. S. Kawasaki. *Photosensitivity in optical fiber waveguides: Application to reflection filter fabrication*. Appl. Phys. Letters 32, 647—649 (1978).

[5] G. Meltz, W. W. Morey, and W. H. Glenn. *Formation of Bragg gratings in optical fibers by a transverse holographic method.* Opt. Lett. 14, 823—825 (1989).

[6] K. O. Hill and G. Meltz. *Fiber Bragg Grating Technology: Fundamentals and Overview.* J. Lightwave Technol. 15, 1263—1276 (1997).

[7] T. Erdogan. *Fiber Grating Spectra.* J. Lightwave Technol. 15, 1277—1294 (1997).

[8] A. Othonos and K. Kalli. *Fiber Bragg Gratings: Fundamentals and Applications in Telecommunications and Sensing.* Artech House, 1999.

[9] A. W. Snyder and J. D. Love. *Optical Waveguide Theory*. Chapman & Hall, 1983.

[10] H. Kogelnik. *Filter response of nonuniform almost-periodic structures*. Bell Sys. Tech. J. 55,109-126 (1976).

[11] D. Marcuse. *Theory of Dielectric Optical Waveguides.* New York Academic 1991.

[12] L. Poladian. *Resonance Mode Expansions and Exact Solutions for Nonuniform Gratings.* Phys. Rev. E 54, 2963—2975 (1996).

[13] R. J. Van Steenkiste and G. S. Springer. *Strain and Temperature Measurement with Fiber Optic Sensors*. Technomic, Lancaster, PA, 1997.

[14] S. W. James, M. L. Dockney, and R. P. Tatam. *Simultaneous independent temperature and strain measurement using in-fiber Bragg grating sensors.* Electron. Lett. 32(12) 1133–1134,1996.

[15] J. S. Sirkis*. Unified approach phase-strain-temperature models for smart structure interferometric optical fiber sensors: part I*. Opt. Eng. 32(4), 752–761, 1993.

[16] P. Sivanesan, J. S. Sirkis, V. Venkat, and Y. Shi*. Simultaneous measurement of temperature and strain using a single fiber Bragg grating.* Proc. ASME/SPIE Conf. on Smart Structures and Materials, Proc. SPIE. 3670**,** 92–103, 1999.

[17] Max Born and Emil Wolf. *Principles of Optics*. Cambridge University Press, 7th ed. 1999.

[18] S.M. Melle, K. Liu and R.M. Measures, *Practical fiber-optic Bragg grating strain gauge system.* Applied Optics, 32(19), 3601-3609, July 1993.

[19] Amnon Yariv. *Coupled Mode Theory for Guided-Wave Optics.* IEEE J. Quant. Elec., QE-9(9), Sept. 1973.

[20] S.W. James, R.P. Tatam, S.R. Fuller and C. Crompton. *Monitoring transient strains on a gun barrel using fiber Bragg-grating* sensors. Meas. Sci. Tech., 10, 63-67, 1999.

[21] S-K Lee, S. Lou, I-C Song, S-H Jeong and B.H. Lee. *Signal processing for strain measurement system with fiber Bragg grating.* Kwangju Inst. Sci. Tech, Korea.

[22] J. Bowlus, G. Bajpai and C. LaVigna. *Smart Gun Barrels with embedded fiber optic sensors.* Techno-Sciences Inc. technical report, 2002.

[23] P.D. Flynn, J.T. Gilbert and E.A. Webster Jr. *A Simple Transducer for detecting projectiles in Gun Barrels*. Frankford Arsenal technical report, 1974.

[24] P. Sivanesan. *Optical Fiber Sensor for simultaneous measurement of distributed strain and temperature*. Dissertation submitted to University of Maryland, College Park, 2002.

[25] K. Broadwater. *Characterization and cure monitoring of epoxy-cured fiber optic connectors via Fiber Optic Sensors*. Dissertation submitted to University of Maryland, College Park, 2001.

[26] G. Wehrle, P. Nohama *et al. A fiber optic Bragg grating sensor for monitoring ventilatory movements.* Meas. Sci. Technol. 12, 805-809, 2001.

[27] G A Johnson and S T Vohra. *Deployment of fiber Bragg grating based measurement system in a structural health monitoring application.* Smart Mater. Struct. 10, 534-539, June 2001.

[28] Luna Innovations Inc. (www.lunainnovations.com)

[29] Amnon Yariv. *Quantum Electronics*. John Wiley and Sons, 3rd edition, 1989.

[30] C. LaVigna, J. Bowlus, H. Kwatny, S. Chen, H. Zhang and S. Cytron. *Performance enhancement and health monitoring of a medium caliber gun system using optical fiber Bragg grating sensors.*

[31] IN-SNEC. (www.in-snec.com)

[32] A. Fernandez Fernandez *et al*. *Multi-parameter force sensing with fiber Bragg grating sensors*. Proc. IEEE/LEOS Symposium, Amsterdam, 2002.